Electronic Thesis and Dissertation Repository

10-24-2012 12:00 AM

Studies in shallow and thin-film flows

MD Mahmuder R. Faisal, *The University of Western Ontario*

Supervisor: Dr.Roger E.Khayat, *The University of Western Ontario*
Joint Supervisor: Dr.Ernest K. Yanful, *The University of Western Ontario*
A thesis submitted in partial fulfillment of the requirements for the Master of Engineering
Science degree in Mechanical and Materials Engineering
© MD Mahmuder R. Faisal 2012

Follow this and additional works at: https://ir.lib.uwo.ca/etd

Part of the Mining Engineering Commons, and the Other Mechanical Engineering Commons

STUDIES IN SHALLOW AND THIN-FILM FLOWS

(Spine title: Studies in shallow and thin-film flows)

(Thesis format: Monograph)

By

Md Mahmudur Rahman <u>Faisal</u>

Graduate Program in Faculty of Engineering

Department of Mechanical & Materials Engineering

A thesis submitted in partial fulfillment

Of the requirements for the degree of

Master of Engineering Science

School of Graduate and Postdoctoral Studies

The University of Western Ontario

London, Ontario, Canada

THE UNIVERSITY OF WESTERN ONTARIO
School of Graduate and Postdoctoral Studies

CERTIFICATE OF EXAMINATION

Supervisor   Examiners

_____
Dr. Roger E. Khayat
                                                        _____
Co-supervisor   Dr. Eric Savory

_____
                                                        _____
Dr. Ernest K.Yanful
                                                        Dr. Liying Jiang
Supervisory Committee

                                                        _____
_____
                                                        Dr. Ralph E. Baddour
Dr. Eric Savory

The thesis by

Md Mahmudur Rahman <u>Faisal</u>

entitled:

Studies in Shallow and Thin-film flows

is accepted in partial fulfillment of the

requirements for the degree of

Master of Engineering Science

_____   _____
         Date   Chair of the Thesis Examination Board

ABSTRACT

The present study examines the influences of surface tension and wind direction in shallow or thin-film flow with the inclusion of inertial effect. In this present study starting with the fundamental equations (conservation of mass and momentum), an analytical method is introduced to determine the bottom stress at different position of a shallow or thin-film flow domain under the influence of oscillatory wind conditions. The novelty of this study is that the viscous and surface tension effects are considered in this study, whereas in most of the existing studies in a shallow or thin-film flow domain (a shallow tailings pond) the viscous and surface tension effects are neglected. A small perturbation method is used to solve the problem, and finally, the expressions for the flow field (elevation, flow velocity and bottom stress) are found as the solution of the problem in a shallow tailings pond. It is observed from the present study that the presence of inertia tends to increase the flow field values while presence of surface tension reduces the values for the flow field. The flow field suggests that surface tension tends to play different role to inertia. Increase in wind angle values reduce the flow field values as due to higher wind angle less wind stress acts over the flow domain. No significant differences are found for different values of inertia, surface tension and wind direction for the flow field at least in appearance, but the magnitude is different for the flow field for high and low values of inertia, surface tension and wind direction. The calculated bottom stress values from the present study without surface tension effect gives the same qualitative and quantitative values as of linear theory and experiment to verify the present study. It is found from the present study that the bottom stress value decreases when the depth in the shallow pond increases.

Keywords: Shallow flow, Oscillatory wind flow, thin-film flow, inertia, surface tension, wind stress, bottom stress.

ACKNOWLEDGEMENTS

The author gratefully acknowledges his advisors Dr. Roger E. Khayat and Dr. Ernest K.Yanful for their invaluable support, guidance and consistent encouragement throughout the course of this work.

The author is thankful to his co-workers especially Omar Bin Yusuf, Rajib Kumar Saha and friends from the *Fluid Mechanics and Polymer Processing Research Laboratory* for their helpful discussions and creating a friendly and enjoyable working atmosphere.

The financial support of the Natural Sciences and Engineering Research Council of Canada (NSERC) and of the University of Western Ontario is acknowledged.

The author is deeply indebted to his parents A.S.M Musfiqur Rahman and Rokeya Begum and siblings for their moral support, sacrifice and encouragement.

TABLE OF CONTENTS

LIST OF FIGURES

NOMENCLATURE

a, b, c   Parameters

A, B, C   Constants

Ca   Capillary number

C_b Bottom friction co-efficient

C_d Wind friction co-efficient

D   Reference length (transverse direction) (m)

Fr   Froude number

g   Gravitational acceleration $\left(m/s^2 \right)$

G   Gravity number

h   Depth of water

H   Depth of water (m)

H_1 Significant wave height (m)

L   Reference length (streamwise direction) (m)

L_1 Significant wave length (m)

n   Normal vector

N	Normal vector
O	Order of
p	Pressure
P	Pressure (Pa)
q	Depth integrated velocity/Flow rate $\left(m^2 s^{-1}\right)$
r	Wind frequency
R	Radius of curvature (m)
Re_D	Reynolds number
s	Tangent vector
S	Tangent vector
t	Time
t	Traction vector
T	Time (s)
T	Excess stress
T_1	Significant wave period (s)
T_{XX}	Stream wise normal stress (N/m^2)

T_{ZZ}	Transverse normal stress (N/m^2)
T_{XZ}, T_{ZX}	Shear stress (N/m^2)
u	Streamwise velocity component
U	Streamwise velocity component (m/s)
U_0	Wind velocity (m/s)
w	Transverse velocity component
W	Transverse velocity component (m/s)
We	Weber number
x	x-axis position co-ordinate
X	X-axis position co-ordinate
z	z-axis position co-ordinate
Z	Z-axis position co-ordinate or the magnitude of elevation
α	Wind direction angle with the positive x-axis (degree)
γ	Surface tension (N/m)
∇	Gradient operator

ε	Perturbation parameter/Aspect ratio
μ	Fluid viscosity $\left(\text{Ns}/\text{m}^2\right)$
ζ	Elevation from the reference level
ρ	Fluid density $\left(\text{kg}/\text{m}^3\right)$
$\boldsymbol{\sigma}$	Total stress
σ	Wind frequency (s)
σ_1	Angular frequency of the wave (s)
τ_{xz}, τ_{zx}	Shear stress
τ_{xx}	Stream wise normal stress
τ_{zz}	Transverse normal stress
τ_s	Wind stress
τ_b	Bottom stress
I	Identity matrix

CHAPTER 1

INTRODUCTION

1.1 **General introduction**

Shallow or thin-film flow is encountered as a fundamental fluid dynamics problem in various realistic settings such as shallow mine tailings pond, flood wave propagation, atmospheric and ocean modelling, hydraulic jump, tides in ocean, dam break wave modelling, paint and surface coatings, chemical and nuclear reactor design etc. The shallow or thin-film flow with free surface displays a variety of interesting dynamics, since the boundary is deformable. In this case, free surface flow problems are challenging because the flow domain is unknown, and the unknown free surface must be determined as a part of the problem formulation. This is in sharp contrast to most of the fluid mechanics problems, where the flow domain and boundaries are known. Thus, for a free surface flow problem, both the flow field and the free surface shape must be determined in space and time. The reason for studying shallow or thin-film flow is to gain understanding of a great range of phenomena (like to predict the bottom stress in a shallow mine tailings pond), which in turn allows making predictions in areas of practical importance.

The Application of thin liquid films is very common in nature and technology so an understanding of their mechanics is very important in many applications. A typical thin-film flow consists of an expanse of liquid partially bounded by a solid substrate with a (free) surface where the liquid is exposed to another fluid (usually a gas and most often air in applications). Thin-film flow is a type of flow, where the thickness (D) in one

direction is much smaller than the characteristic length scale (L) in the stream wise direction. The flow takes place predominantly in the direction of the longer dimension. Thin-film or shallow flow are the same type of flows and they represent similar flow characteristics. In the present study we have mainly dealt with shallow flow. The influence of inertia, surface tension are examined in this study as from the existing literature (O'Brien & Schwartz 2002, Myers 1998, O'Brien & Van Den Brule 1989), it is found that surface tension is important in small scale and thin-film flow and for capillary waves. Surface tension is also important in porous media and oil medium due to the small capillary number values (http://en.wikipedia.org/wiki/Capillary_number) in these mediums. Several studies (O'Brien & Schwartz 2002, Myers 1998, O'Brien & Van Den Brule 1989) have demonstrated that surface tension is important in thin-film and shallow flow and it cannot be neglected in thin-film and shallow flow. Now we will concentrate our study on shallow flow to determine the bottom stress in a shallow tailings pond.

The study of shallow or thin-film flow is of interest in connection with the shallow mine tailings pond, atmospheric and ocean modelling, hydraulic jump, tides in ocean, dam break wave modelling etc. Shallow flow (long wave) is a type of flow, where the horizontal dimension is much larger compared to the vertical dimension. Examples include the ocean, large estuaries, shallow mine tailings pond, seasonal floods; liquid coatings, lubricating films, and on automobile windshields. Pressure distribution is assumed hydrostatic in shallow water flow. The main driving force to cause resuspension in a shallow pond is the oscillatory wind. The horizontal velocity is assumed not to change in the vertical direction that means the flow velocity is independent upon the height of the shallow pond. Figure (1.1) shows the typical shallow flow, where the horizontal dimension

(L) is much larger compared to the vertical dimension (D). The free surface is given by $Z = H(X, T)$ in this figure, where X and Z represent the horizontal and vertical direction of the flow domain.
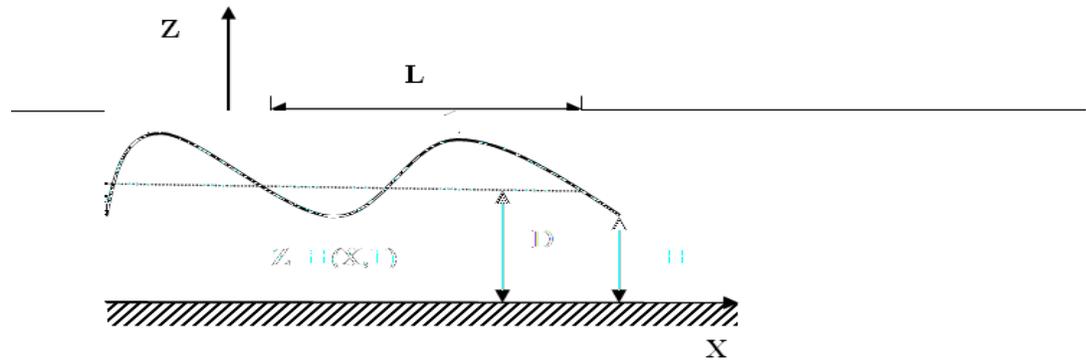
Fig1. 1 Schematic of typical shallow or thin-film flow

In aquatic basins such as shallow lakes, reservoirs and coastal regions, flows are generally shallow water flow, which is driven in most of the cases by shear stresses imparted to the free water surface by the wind, by tide-induced water level variations at the boundaries or by the atmospheric pressure gradient. The governing equations for any fluid consist of field equations resulting from the conservation laws and the constitutive equations. In general, the solution of the thin-film or shallow water equations requires solving the Navier-Stokes equations. It is generally accepted that the unsteady flow of water in a two-dimensional space may be described by the thin-film or shallow water equations, which represent the mass and momentum conservation and can be obtained by the depth averaging of the Navier-Stokes equations in the vertical direction. If the flow is shallow enough than the vertical accelerations can be neglected, then it can

be shown that a good approximation to the flow is to replace all of the flow variables by their averages in the vertical direction. The most interesting cases involve a top fluid surface that is free to exhibit the wave phenomenon. Depth-averaged approximations are probably the best known and most widely used in applications relating to the oceans or other large, shallow bodies of water. In this context, the approximation is most often referred to as the shallow-water or thin-film approximation.

The present study is focused on the shallow flow of an incompressible fluid. The shallow pond is assumed to be small and wind is the main driving force in the flow field. The flow behaviour is examined in this study under the oscillatory wind condition. Moreover, the influences of inertia, surface tension and wind direction on the flow field are examined in this study. In contrast to existing experimental (Yanful and Catalan 2002) and theoretical (linear wave theory) studies, the effect of surface tension has been included in this study and the fluid is assumed to be viscous in this study. The presence of surface tension in a fluid is expected to alter the flow characteristics. In order to obtain an analytical solution, a number of assumptions are made regarding the shape of the pond and the type of wind stress, and simplifications are made to the governing equations. This at some extent limits the use of the solution, when considering the real world problems.

1.2. Relevance to reality

The Application of thin-films and shallow flows are very common in nature and technology so an understanding of their mechanics is very important in many real life problems. In this present study we are interested to deal with shallow flow to determine the bottom stress under the influence of periodic wind stress over the flow domain. The present work is of fundamental importance given the significant quantitative role that bottom stress plays to cause erosion and resuspension in a shallow mine tailings pond. Therefore, prediction of the bottom stresses in a shallow mine tailings pond is studied in this study. In general, surface tension has been neglected in most of the studies of shallow water flow. This can be quite reasonably justified, since in most practical applications of shallow flow, surface tension is relatively small. However, there may be still some applications in which surface tension plays a significant role. That is why the problem is formulated with and without the effect of surface tension to see the effect of surface tension on the flow field.

From the existing studies, it is understood why it is important to predict the bottom stress in shallow water flow, compared to the prediction of the bottom stress in deep water flow. Bottom stress is an important parameter to predict and it contributes significantly for the resuspension in shallow water flow compared to deep water flow. In deep water particles near the surface move in circular path making ocean surface wave a combination of longitudinal (back and forth) and transverse (up down motions) motion. When wave propagates in shallow water flow the particle trajectories are compressed into ellipses. So, in shallow water flow there is only back and forth motion at the bottom and the influence of bottom is dominant to cause resuspension compared to deep water flow.

This phenomenon is schematically represented in figure (1.2), where point A represents the position of fluid particle at deep water flow. In this case, the orbital motion of fluid particle decreases rapidly with increasing depth below the free surface. On the other hand, in shallow water flow the elliptical movement of a fluid particle is observed at the bottom of the flow domain (point B represents the bottom position in shallow water flow). Point 1 represents the propagation direction of the flow and (2, 3) represent crest and trough of the flow domain respectively.
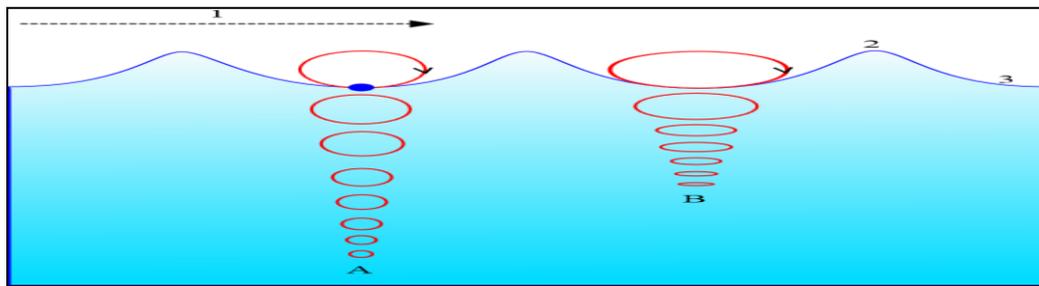
Fig1. 2 Motion of a particle in an ocean wave (**http://en.wikipedia.org/wiki/Wave_power**)

There are some differences in the characteristics of shallow water and deep water flows. Waves in shallow water flow are strongly influenced by the presence of the bottom compared to deep water flow. Circular orbit is observed for deep water flow and its influence is less dominant at the bottom to cause resuspension. On the other hand, in shallow water flow, as waves are influenced by the bottom more, the interaction alters the orbital shape from circular to elliptical and strong erosion is observed in this case compared to deep water flow. This behavior and characteristics of shallow water flow is represented in figure (1.3). In this figure, it is shown that in deep water flow wave action

decreases rapidly with depth, while in shallow water flow wave action does not decrease with depth. In shallow water, there is only longitudinal motion at the bottom while longitudinal as well as transverse motions for deep water flow.
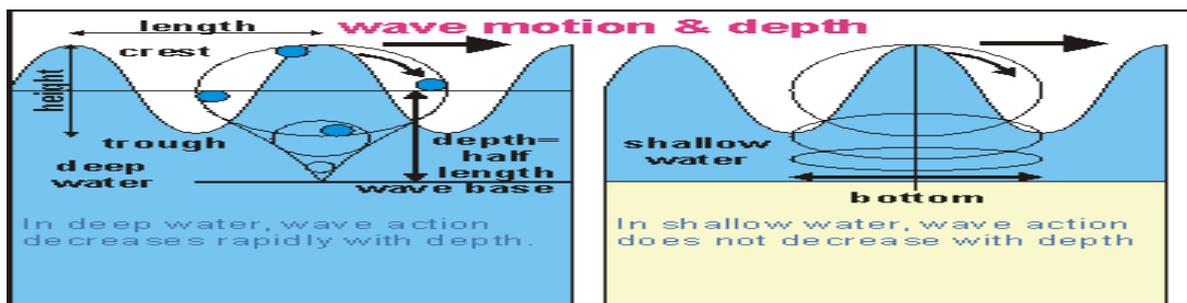
Fig1. 3 Flow orbit at the bottom in shallow and deep water flows

http://www.seafriends.org.nz/oceano/waves.htm

In shallow water flow, where depth is less than one-half of the wavelengths, orbits are progressively flattened with depth, and there is little wave drift. Water just above the seafloor cannot move in a circular path and can move only back and forth. Figure (1.4) demonstrates the variation of the flow behavior and characteristics (wave celerity, wave
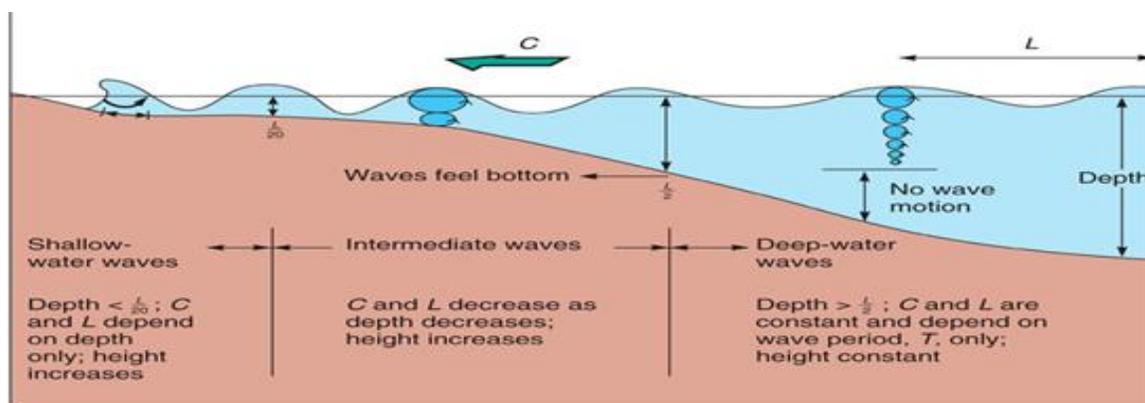
Fig1. 4 Flow behavior moving from deep water flow to shallow water flow

length), when the waves are moving from deep water flow to shallow water flow through intermediate flow. It is observed from the figure, as the flow moves from deep water flow to shallow water flow, wave orbit changes from circular to elliptical shape.

Mining of metal and uranium ores produces large amounts of reactive sulphide mine tailings which are serious threats and concerns to the environment. One of the approaches used for environmental management of the tailings is the use of shallow water covers, typically up to 2 m. As oxygen is one of the key factors in the oxidation of
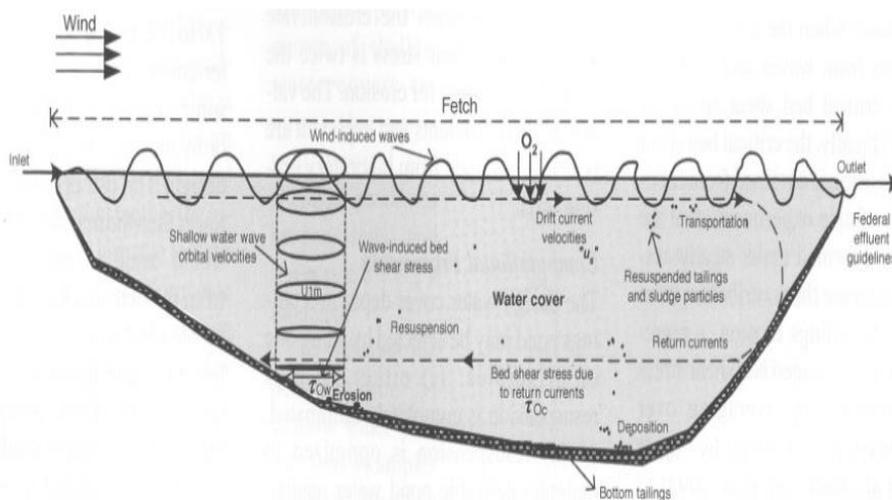
Fig1. 5 Schematic representation of tailings pond hydrodynamics (Yanful, E.K., Samad M. & Mian, M.H. (2004))

reactive sulphide minerals present in the tailings, water covers do provide an important control measure. Due to the low diffusivity and solubility of oxygen in water (2e-9 m^2/s and 8.6 g/m^3 at $25°C$) compared to the correspondingly higher values in air (1.78e-5 m^2/s and 285 g/m^3), oxygen transport by molecular diffusion is too slow to be of any

significance in the oxidation of sulphide mine waste (Simms et al. 2001). Water covers can, therefore, be an effective choice in reducing tailings oxidation and resuspension.

Mine tailings ponds are normally designed to minimize the wind-induced bottom erosion and sediment resuspension. Figure (1.5) shows the representation of a tailings pond hydrodynamics. In this figure, the formation of the wind induced bed shear stress and bed shear stress due to return current is illustrated. This figure also shows the wind action over the flow domain, which induces bottom stress to cause resuspension of the tailings. The ponds are constructed with a minimum depth of water cover.

Deep water covers appears to be less attractive option to mine operators due to concerns on the long-term stability of reservoirs from hydrostatic pressures, the high costs of construction including efficient flood control systems and its maintenance, and the attendant monitoring of the structure and water quality (Yanful, et al, 2004). Shallow water covers, compared with deeper ones can also provide the twin benefits of limiting oxygen diffusivity and solubility, thus dampening AMD production and metals release. For shallow water flow, wave action is the dominant force in creating shear while it is the return current in deep water flows.

A major problem with implementing a water cover over tailings is the presence of the strong wind-induced waves and currents in water. Wind waves deliver energy to the water to generate currents and initiate sediment motion. When wind blows over water, it exerts a shear stress on the water surface. Although the wind shear stress is usually very small, its effect, when integrated over a large body of water, can be catastrophic (Dean and Dalrymple, 1991).

1.3 Literature review

Thin-film flow has mostly been examined for Newtonian fluids (Brourgin 1997; Kistler & Schweizer 1997). Generally most studies involve either gravity driven or surface-tension-driven flow. A simple and obvious example of thin-film flow is the flow of a (thin) raindrop down a windowpane under the action of gravity. Typically, the flow velocity in directions perpendicular to the substrate (the window-pane) is much smaller than the main flow velocity along the windowpane. The most suitable approach for modeling such flows is via the momentum equation (the Navier-Stokes equations in the case of a Newtonian liquid). The approach taken here will be to exploit the existence of the small aspect ratio ($\varepsilon = \dfrac{D}{L}$) to expand the solution in a perturbation series in powers of ε. In doing so thin-film or long wave approximation is developed (Benney 1966) with the advantage that analytic solutions will often be possible and where this is not feasible, the reduced numerical problem will be greatly simplified (Tuck & Schwartz 1990). The approximation has much in common with classical lubrication theory (Acheson 1990) and is thus also referred to as the lubrication approximation. In the next section some previous studies on surface tension driven thin-film flows are described.

In many practical thin-film models, surface tension plays a significant role (O'Brien, Van Den Brule 1989). Even when formally small, surface tension often has a significant smoothing effect preventing the formation of shocks. Mathematical models are described for flows on flat and curved surfaces including other effects such as gravity, surface tension and inertia. Asymptotic derivations of lubrication theory for 2-D

problems with a free surface are given by Benney (1966) without surface tension and by Atherton and Homsy (1976) where surface tension is included.

In Encyclopedia of Surface and Colloid Science (2002) by O'Brien & Schwartz , it was described that it is the common practice of many authors to rescale the surface tension terms so that they are O (1), by assuming that $\varepsilon^3 / Ca = O(1)$, (where Ca is the capillary number). It was assumed whether the rescaling is technically correct depends on the particular parameter values in the problem under consideration but the idea is that even if these terms are everywhere small, including them will still give a correct approximation to leading order. This approximation usually has the desirable effect of making the numerical technique more stable. The study was more concerned with the flow on centimeter-scale objects rather than meter-scale objects.

Myers (1998) has described the work on thin-films, where surface tension is a driving mechanism. The highlight of this paper is the substantial amount of literature dealing with relevant physical models and also analytic work on the resultant equations. Thin- film flows driven by surface tension have been shown to describe a diverse range of physical situations and lead to many mathematical problems. This paper highlights the wide range of situations in which surface tension drives a thin-film flow. Free films, such as a single soap film, have two free surfaces but the governing equation may be reduced to that of shear flow if one or both of these surfaces are saturated with surfactant. Otherwise higher-order approximations to the Navier-Stokes equations are required.

Stone (2002) has demonstrated that waves in thin-films or shallow flow behave differently than waves in deeper flow. This is because of the high viscous stresses, low impact of inertial forces as the lubrication assumption remains the basis for the simulation of thin-film flow where the inertial effects are neglected (Mazouchi & Homsy 2001), low velocity, and influence of surface tension at the small scales involved. In this paper, the governing equations of thin-films are derived from the Navier-Stokes equations. The behavior of thin-films can be described by the lubrication approximation. This approximation was used to find the behavior of small disturbances as they evolve in space and time. In order to extend the results to faster waves and deeper liquid, inertial terms should be included as inertial effect is important in deeper liquid. By doing this, one could check that the behavior approaches the well known behavior of waves in deeper liquids. Stone considered the time-dependent motion of thin-films in cases where viscous effects are significant. This topic may be considered naturally under the theme "reactive flows" since changes in surface tension produce fluid motions this is a response that occurs at fluid-fluid interfaces.

Kalliadasis, Bielarz & Homsy (2000) have described the problem of the flow over a trench under the action of an external body force, solving the assumed governing one-dimensional long wavelength, or lubrication approximation numerically as a means of analysing further the case of trench depths comparable with, or larger than, the associated unperturbed film thickness. They have considered the slow motion of a thin viscous film flowing over a topographical feature (trench or mound) under the action of an external body force. Using the lubrication approximation, the equations of motion were simplified to a single nonlinear partial differential equation for the evolution of the free surface in

space and time. They have also explored the effect of gravity, showing that it could result in the disappearance of capillary ridges. The stability of the latter was considered in a subsequent article by Kalliadasis & Homsy (2001).

Mazouchi & Homsy (2001) have compared the solution of the two-dimensional flow to their earlier thin-film based solution. This comparison indicated that the thin-film hypothesis remains valid even in the presence on steep topographic variation. Mazouchi & Homsy (2001) attributed this validity to the smoothing role that surface tension effects tend to play. Their study was limited, however to surface-tension dominated inertia less flows.

In the paper of Gaskell et al. (2004), a range of two and three-dimensional problems is explored featuring the gravity-driven flow of a continuous thin liquid film over a non-porous inclined flat surface containing well-defined topography. These are analyzed principally within the framework of the lubrication approximation, where accurate numerical solution of the governing nonlinear equations is achieved. The accuracy of the lubrication approximation in the context of such topographies is assessed and quantified by comparison with the solutions of the full Navier-Stokes equations. The Navier-Stokes solution also illustrates the effect of Reynolds number on the capillary through and the two-dimensional flow structures caused by steep topography. Most previous investigations have concerned thin-film flows over two dimensional topographies. Important early examples are the combined theoretical and experimental studies of Stillwagon & Larson (1988) and Pritchard, Scott and Tavener (1992). Both sets

of authors demonstrated lubrication theory to be surprisingly accurate for modelling purposes even for cases where it is not strictly valid, as for the flow over shallow trenches.

Siddique and Khayat (2002) have shown that in classical lubrication theory the Navier–Stokes equations are reduced to the Reynolds equation under the assumption that the inertia forces are negligible compared to the viscous forces. This conventional thin-film theory is valid for small Reynolds number flow. They also addressed that recently, owing to some practical applications, the need to include inertia effects has arisen because of the increasing number of lubrication problems that involve moderately large Reynolds number.

From the existing literatures described above, it is found that surface tension plays a significant role in thin-film or shallow flow. That is why the problem is formulated with the inclusion of surface tension to see the influence of surface tension on the flow field. The study is done at a moderately large value of Reynolds number to see the influence of inertia as well as surface tension on the flow field. In most of the existing studies on thin-film or shallow flow, inertial effects are neglected (Mazouchi & Homsy 2001) or assumed low inertia flow. The objective of the present study is to determine the bottom stress in any shallow or thin-film application with the inclusion of viscous and surface tension forces, where wind is the main driving force to initiate the motion. The present study is applicable for any thin-film or shallow flow to determine the bottom stress under the influence of moderately Reynolds number and surface tension. Now we will focus on shallow flow or more precisely on a shallow tailings pond to determine the bottom stress

under the influence of viscosity and surface tension at a moderate Reynolds number. Some literatures on the bottom stress determination in a shallow mine tailings pond are discussed in the next section.

The study of resuspended flooded mine tailings pond has been extensively examined previously in the literature. However, fundamental work on this analysis is limited. In addition, most published work on prediction of the bottom stress for reactive sulphide rich tailings pond is based on empirical, predictive methods. Most studies focused on Airy (linear wave) theory to predict the flow behavior in the shallow mine tailings pond. There are many studies devoted to the modeling and simulation of the resuspended flooded mine tailings. Most importantly, resuspension in mine tailings pond has been predominantly examined from the empirical methods (Samad and Yanful 2005), (Yanful and Catalan 2002) and to a much lesser extent from the fundamental fluid equations (conservation of mass and momentum) considering the viscous and surface tension effects.

Generally, for prediction and field measurement of flooded mine tailings (Yanful and Catalan 2002), linear wave theory is often used. According to Bengtsson et al. (1990), it is usually sufficient to use the linear wave theory in small lakes. At first glance, this theory appears to be a suitable choice for modeling the flow behavior in shallow mine tailings pond. However, the linear wave theory assumes the fluid to be inviscid (where viscosity, drag and friction terms are negligible). Moreover, the flow becomes seriously limited in the presence of ambient velocity (current) and high amplitude waves. This theory also excludes the effect of surface tension (which includes the exclusion of

capillary waves and other very short waves). This theory is only applicable for a smooth and impermeable bottom. Therefore, the limitations of this theory sometimes limit its use in the real world problems.

Wind induced bed shear stress in a closed water body is made of two parts (i) bed shear stress due to waves and (ii) bed shear stress due to circulatory currents. However, it is not clear from the published literature how the waves and currents should be handled in enclosed shallow water bodies to obtain the total bed shear stress exerted on the bed surface by the wind action, which is required for analyzing resuspension and sediment transport processes. In many studies the current induced bed shear stress in shallow water is either considered too small to contribute to resuspension (Luettich et al. 1990; Bailey and Hamilton 1997; Cozar et al. 2005) or estimated using theoretical and empirical approaches developed under laboratory conditions such as those developed by Wu and Tsanis (1995) and Yang (2001). Previous studies (Yanful and Catalan 2002) ignored the current induced bed shear stress in a tailings pond, assuming it to be only 10% of the total bed shear stress. However, Samad and Yanful (2005) later found that the bed shear stress due to currents often exceeded 20% of the total bed shear stress. In their study, they also calculated total bed shear stress as a linear addition of both wave and current induced bed shear stresses.

Quick et al. (1987) noted that linear addition of wave and current, parts of the total bed shear stresses is a simplification of a rather complex process. In other studies, it has been reported that the wave and currents should not be treated separately and their interaction may increase the total bed shear stress (Grant and Madesn 1979; Jing and

Ridd 1996; Jin and Ji 2004). In order to include wave-current interaction in the total bed shear stress calculations, actual field measured current data is needed. In most of the tailings pond studies, information about actual currents data have been missing and currents were empirically calculated as counter currents.

In most studies so far conducted on the tailings ponds, the total bed shear stress was taken as a simple linear addition of the shear stress contributions from waves and currents (Yanful and Catalan 2002; Samad and Yanful 2005; Kachhwal et al. 2010). In these studies near bed, currents were assumed as counter current flow in opposite direction to wind based on the Wu and Tsanis (1995) theoretical model developed for pure currents in absence of waves. In the presence of both waves and currents, linear addition may not be accurate especially for strong currents and may underestimate the total bed shear stress. The empirical approaches used to estimate the wind induced currents in these tailings pond studies do not provide any information on current directions and circulation patterns. The lack of field measured wind induced current data in small tailings pond is a constraint. Kachhwal (2011) measured real time wind induced currents in a tailings pond and studied the effect of wave-current interaction on total bed shear stress. It is clear from his results that currents significantly contribute to total bed shear stresses to cause resuspension in a tailings pond.

The tendency of wind-induced waves to erode and resuspend mine tailings has been investigated by Yanful and Catalan (2002) using published semi empirical predictive methods (United States Army Coastal Engineering Research Center, 1984), where they have calculated the wave characteristics wave height, wave length and wave period associated with the observed winds. They also measured critical shear stress of the

tailings, and sediment trap measurements at the Heath Steele Upper Cell tailings pond, New Brunswick, Canada. The prediction of resuspension is compared to the field measured resuspension of tailings under varying water cover depth at a site based on the results, it is concluded that bed shear stress was higher in shallower water covers. Under the maximum sustained wind speed of 10 m/s observed at the study site, the predicted total shear stress exceeded the upper and lower bounds of the critical shear stress in parts of the tailings pond, where the water cover was less than 1.18m and 1.34 m deep, respectively. By comparison, field measurements of tailings resuspension using sediment traps suggested that resuspension occurred primarily in areas where the water cover depth was 1 m or less.

The study by Mian and Yanful (2003) has demonstrated the variation of the wave heights with wind-induced waves. The idea of the significant wave height is useful in determining the bottom shear stresses. Mine tailings would resuspend due to the bottom shear stresses that are greater than the critical shear stresses required for the tailings resuspension. It was observed that the shear stresses exceeded the critical shear stresses required for erosion of the bed tailings at wind speeds higher than 9 m/s. Analysis of the wind data demonstrated that hourly averaged wind speeds exceeded 9 m/s quite frequently at the two sites, and that resuspension likely occurred. Based on the results of the resuspension measurements and tailings particle size distribution, it was assessed that resuspension is not only a function of depth and wind generated stresses, but also depends on other factors, such as cohesion and self-consolidation of the tailings, and the topography of the site. They also discussed that although the SMB equations may have been used to select minimum water-cover depths at the two tailings sites, resuspension

was still observed at these sites as already discussed. Thus, it might be inferred that, even with the use of SMB equations for the design of water covers for new mine-tailings sites, resuspension might still be expected at higher wind speeds, leading to oxidation and potential deterioration of water quality.

Rodney and Stefan (1987) have presented a conceptual hydrodynamic model of wind effects in settling pond. Three wind generated hydrodynamic processes (wind generated currents, progressive wave and standing wave) have been identified as contributing to the resuspension of bed sediment in a shallow pond. They also tried to derive and verify a relationship between the bed shear stress and the resuspension rate. They concluded that it was necessary to examine the methodology for relation of the bed erosion rate to the shear stress that is directly applicable to the pond sediment.

1.4 Motivation:

Generally, thin-film and shallow flow problems are reduced to one dimension by implementing the lubrication approximation. Although the lubrication assumption remains the basis for the simulation of thin-film flow, it is mostly used with inertial effects neglected (Mazouchi & Homsy 2001). Recently, owing to some practical applications without free surface as high speed film casting, large size bearing and with free surface as industrial dip coating, film-coating, dam break wave modelling; the need to include inertia effects has arisen because of the increasing number of thin-film or shallow flow problems that involve moderately large Reynolds number (Oron, Davis & Bankoff 1997, Venkatesan & Shivpuri 1995, Kizito, Kamotani & Ostrach 1999, Ruschak & Weinstein 2000). From the existing studies (O'Brien & Schwartz 2002, Myers 1998, O'Brien & Van Den Brule 1989, Atherton & Homsy 1976), it is found that surface tension plays a significant role in thin-film or shallow flow. That is why the problem is formulated with the inclusion of surface tension to see the influence of surface tension on the flow field. The study is done at a moderately large value of Reynolds number to see the influence of inertia as well as surface tension on the flow field. Therefore, the objective of the present study is to examine the influences of surface tension and wind direction in shallow or thin-film flow with the inclusion of inertial effect. The formulation and simulation are carried out for a two-dimensional thin-film and shallow flow in order to better understand the intricate flow structures of thin-film and shallow flow. The present study is undertaken to observe the effect of surface tension at a moderately high Reynolds numbers (inertia effects are considered) in thin-film and shallow flow.

For small inertia flow of a Newtonian film, Benney's (1966) long wave (LW) approximation is often used. At first glance, the LW approximation appears to be a suitable choice for the modeling of thin-film or shallow flow. However, the LW approximation becomes seriously limited in the presence of moderate or high inertial effect (Chang 1994). For a Newtonian film, the LW approximation at Re >> 1 is typically not valid, and it is generally found that in this case, inertial effects are better represented using the boundary-layer (BL) formulation. In this present study, boundary-layer formulation is found using the suitable scaling for typical shallow flow. The present study is considered for moderately large inertial effects.

Free surface and interfacial flows are inherently complicated because of the unknown position of the free surface or interface, which must be determined as a part of the problem. The understanding of the thin-film or shallow flow initiated by the wind action remains challenging, despite the continuous development of new solution techniques and the advent of powerful computational platforms due to the fact that computational domain is unknown a priori along with the unknown position of the free surface. So it is quite challenging to assume the correct boundary conditions to solve the problem.

The bottom velocity expression calculated from the linear theory for a typical shallow tailings pond neglected the viscous and surface tension forces whereas in this present formulation the fluid is assumed to be viscous and the influence of surface tension is considered at a moderate inertial effect. In linear theory formulation the lateral boundary conditions are assumed periodic with position and time as the boundaries are not fixed or confined while in the present formulation no-penetration conditions are

assumed at the both lateral boundaries as the flow domain is assumed confined and fixed. The bottom boundary condition remains the same in the present formulation as of linear theory that the flow velocity at the bottom is zero due to no- penetration condition in the transverse direction.

Yang et al. (2008) have described an engineering model for countercurrent flow under wind induced waves and current. They have shown that the flow structure in closed bodies of water subjected to surface shear and waves remain poorly understood. They have addressed that the wind-generated waves in typical closed water bodies are either deep or intermediate and man-made shallow water covers used by the mining industry to isolate reactive mine tailings from the environment typically operate under intermediate-water conditions. Their proposed engineering model is capable of representing cases of wind/wave-driven countercurrent flows but they recommended that further study is required to determine if the model parameters are universal or if they require adjustment for different flows conditions. Most early efforts to investigate such flows focused solely on the surface drift driven by wind and waves. Laboratory studies by Wu (1968), Plate (1970) and Spillane and Hess (1978) made progress in the understanding of wind-induced surface drift in confined water bodies. These studies focused on the wind-induced surface motions under fairly small wind generated waves (deep-water conditions), but in the present formulation we have focused our studies on shallow water conditions. The study has shown that for typical wind-water interactions, the flow field is normally fully turbulent whereas in our model the flow field is assumed laminar under the periodic wind stress. As the flow domain in assumed laminar in our model, we have neglected the countercurrent or return flow in the flow domain. In the model of Yang et al. the fluid is

assumed to be viscous but the surface tension effect is neglected while in our formulation we have considered the surface tension as well as viscous effect in a shallow or thin-film domain.

In the present model the wind is taken at an angle (α) with the x-axis of the flow domain. But in most of the existing studies (Fenton 2010, Matthews et al. 1996, Lick 1976) it is found that, wind acts parallel over the shallow flow domain. Although in most of the existing studies (Lick 1976, Fenton 2010) the angle is taken as zero $(\alpha = 0)$ but in this present study using wind at an angle (α) is described as an alternative way of describing wind condition over the shallow pond which resembles with the existing wind stress expression when the angle is zero. Although we have tried to compare our results with the existing linear theory results but the wind situation in two cases are not same. As in linear theory, wind is taken as constant while in our model we have assumed periodic wind stress with time. But if we assume the wavelength to be infinite then the wind condition in our formulation can be assumed constant as of linear wave theory. We have tried to find a behavioral trend of the bottom stress for different water depth in a tailings pond.

Now for a typical shallow tailings pond, the main focus of the present study is to predict the bottom shear stress in a shallow tailings pond. The focus is concentrated on bed shear stress due to wind induced waves, as it is found from the literature that the bed shear stress due to return current is too small (Luettich et al. 1990; Bailey and Hamilton 1997; Cozar et al. 2005) compared to the bed shear stress due to wind induced waves. Therefore in this present study bed shear stress due to return current is neglected. Two

cases are considered in this study, with and without the effect of surface tension on the flow field. The influences of surface tension, inertia and wind direction on the flow field are explored in this present study. Most published work (Yanful and Catalan 2002, Samad and Yanful 2005) on prediction of the bottom stress for tailings pond is based on empirical, predictive methods where the linear theory is used to predict the flow behavior in a shallow tailings pond.

The main focus of this present study is to predict the bottom stress starting from the fundamental equations (conservation of mass and momentum) for a given wind speed and water depth in the presence of inertia and surface tension in a tailings pond. Starting with the fundamental equations, the equations are converted to boundary-layer equations for shallow water flow using the suitable scaling method. Insertions of the effect of ambient wind condition and bottom shear stress are done to formulate the problem for the flow field. A small perturbation method is used to solve the problem and finally, the expressions for the elevation, flow velocity and bottom stress are found as the solution of the problem. The predicted bottom stress values from the present study using different water depths for a particular wind velocity, show good agreement with the existing theoretical (linear theory) and the experimental (Yanful and Catalan 2002) bottom stress values although the wind condition in the present model is not same as of linear theory.

The characteristics and applications of shallow or thin-film flow are described in this chapter. Some previous studies on thin-film flow where surface tension was considered are also described in this chapter. As we are mainly focusing our attention in shallow flow, so previous studies of the resuspended flooded mine tailings ponds in the

literature are also described in this chapter. This chapter has demonstrated the significance of the present study as well as relevance of the present study to reality. Moreover, it describes how this study can be an alternative choice for predicting the bottom shear stress in a shallow mine tailings pond considering the viscous and surface tension effects. This chapter describes the significance of the bottom stress in shallow water flow compared to deep water flow. The benefits and significances of shallow water covers compared to deep water covers are also illustrated in this chapter.

CHAPTER 2

GENERAL PROBLEM FORMULATION

In this chapter, the governing equations are introduced, including the suitable scaling of the constitutive equations as well as the boundary conditions for shallow water flow. The solution procedure is also described in this chapter in some detail.

2.1 Problem formulation and boundary conditions for shallow water flow

The fluid examined in this study is assumed to be an incompressible fluid, which has the fluid properties of density ρ and viscosity μ. The problem is examined in the (X, Z) plane. Regardless of the nature of the fluid, the continuity and the momentum conservation equations must hold. For an incompressible fluid, the conservation equations are:

$$\nabla \cdot \mathbf{U} = 0, \tag{2.1.1}$$

$$\rho\left(\mathbf{U_T} + \mathbf{U} \cdot \nabla \mathbf{U}\right) = \nabla \cdot \boldsymbol{\sigma} - \rho \mathbf{g}, \tag{2.1.2}$$

where $\mathbf{U}$ is the velocity vector, $\boldsymbol{\sigma}$ is the total stress, $\mathbf{g}$ is the acceleration due to gravity, T is the time and ∇ is the gradient operator. The total stress is expressed as $\boldsymbol{\sigma} = -P\mathbf{I} + \mathbf{T}$, where $\mathbf{I}$ is the identity matrix; P is the hydrostatic pressure and $\mathbf{T}$ is the excess stress.

Consider the fluid flow in figure (2.1), where X axis represents the horizontal direction and Z axis represents the transverse direction of the flow domain. The free surface is given by $Z = H(X, T)$. The unit normal and unit tangent vector acting on the free surface

is denoted by **n** and **s**. Equations (2.1.1-2.1.2) for conservation of mass and momentum are expressed in dimensional form as
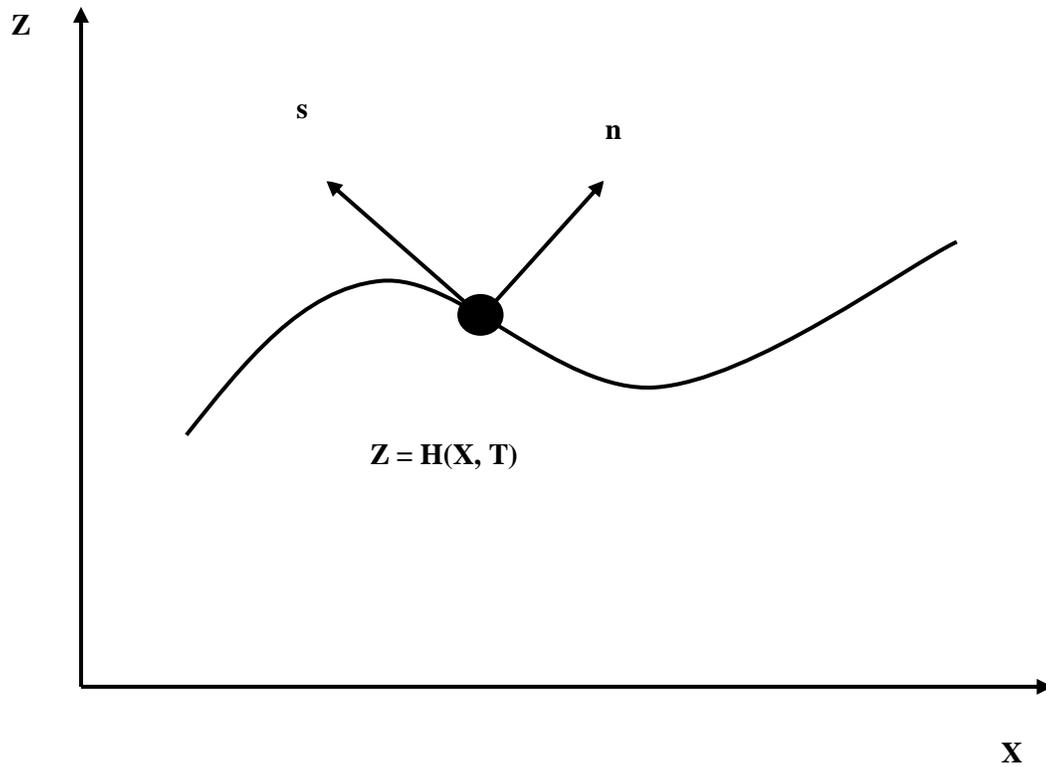
Fig: 2.1 Schematic of the flow domain showing the free surface, normal and tangent vector at the free surface and the horizontal(X) and vertical direction (Z) of the flow domain.

$$\frac{\partial U}{\partial X} + \frac{\partial W}{\partial Z} = 0, \tag{2.1.3}$$

$$\rho\left(\frac{\partial U}{\partial T} + U\frac{\partial U}{\partial X} + W\frac{\partial U}{\partial Z}\right) = -\frac{\partial P}{\partial X} + \frac{\partial T_{XX}}{\partial X} + \frac{\partial T_{ZX}}{\partial Z}, \tag{2.1.4}$$

$$\rho\left(\frac{\partial W}{\partial T} + U\frac{\partial W}{\partial X} + W\frac{\partial W}{\partial Z}\right) = -\frac{\partial P}{\partial Z} + \frac{\partial T_{XZ}}{\partial X} + \frac{\partial T_{ZZ}}{\partial Z} - \rho g, \tag{2.1.5}$$

where all the terms are in dimensional form. Here, U and W are the stream wise (X direction) and vertical (Z direction) velocity respectively and P is the hydrostatic pressure in the shallow pond. Free surfaces occur at the interface between two fluids, such interfaces require two boundary conditions to be applied (i) A kinematic condition which relates the motion of the free interface to the fluid velocities at the free surface and (ii) a dynamic condition which demonstrates the force balance at the free surface.

If the free surface is given by $f = f(X, Z, T) = 0,$ then its normal is given by $\mathbf{N} = \nabla f$ and the unit normal is given by $\mathbf{n} = \pm\frac{\nabla f}{|\nabla f|}$, the plus and minus signs correspond to $\mathbf{n}$ pointing away from and toward the free surface, respectively. In this formulation, it is taken as $\mathbf{n} = +\frac{\nabla f}{|\nabla f|}.$

Now, for this problem the free surface is given by $Z = H(X, T) \therefore f = Z - H(X, T),$ so $\nabla f = -H_X \mathbf{i} + \mathbf{k},$ where $\mathbf{i}$ and $\mathbf{k}$ represents the unit vector in X and Z direction of the flow domain. So, the unit normal vector is expressed as

$$\mathbf{n} = n_X\mathbf{i} + n_Z\mathbf{k} = -\frac{H_X}{\sqrt{H_X^2+1}}\mathbf{i} + \frac{1}{\sqrt{H_X^2+1}}\mathbf{k}. \tag{2.1.6}$$

As the unit tangent vector remains at 90 degree angle to the unit normal vector, therefore, the expression for the unit tangent vector becomes

$$\mathbf{s} = s_X\mathbf{i} + s_Z\mathbf{k} = n_Z\mathbf{i} - n_X\mathbf{k} = \frac{1}{\sqrt{H_X^2+1}}\mathbf{i} + \frac{H_X}{\sqrt{H_X^2+1}}\mathbf{k}. \tag{2.1.7}$$

The dynamic boundary condition requires the stress to be continuous across the free surface which separates the two fluids (air and water). The traction exerted by one fluid (1) on another fluid (2) is equal and opposite to the traction exerted by fluid (2) on fluid (1). As surface tension is included in this study, the dynamic boundary condition is also modified and traction at the free surface is given by

$$\mathbf{t} = -\gamma\kappa\mathbf{n}, \tag{2.1.8}$$

where $\mathbf{t}$ is the traction vector at the free surface, γ is the surface tension and $\mathbf{n}$ is the unit normal vector at the free surface. Note that, the curvature can be positive or negative. It is known that the (κ) is the reciprocal of the radius of curvature (R) and expressed as

$$\kappa = \frac{1}{R} = -\frac{H_{XX}}{\left(1+H_X^2\right)^{\frac{3}{2}}}. \tag{2.1.9}$$

Now, the traction at the free surface in the tangential direction is found by taking the scalar product of the traction with the unit tangent vector to the free surface. Using

equation (2.1.8), the scalar product of the traction vector with the unit tangent vector at the free surface gives

$$\mathbf{t} \cdot \mathbf{s} = -\gamma \kappa \mathbf{n} \cdot \mathbf{s}. \tag{2.1.10}$$

As the unit normal and the unit tangent vector remains perpendicular to each other, their scalar product is zero. $\mathbf{n} \cdot \mathbf{s} = 0$. Using this value in equation (2.1.10) leads to

$$\mathbf{t} \cdot \mathbf{s} = 0, \tag{2.1.11}$$

where $\mathbf{t}$ is the traction vector at the free surface and it is substituted by the scalar product of the total stress $\boldsymbol{\sigma}$ and the unit normal vector. In other words, $\mathbf{t} = \boldsymbol{\sigma} \cdot \mathbf{n}$, using this expression into equation (2.1.11) reduces to

$$\left(\boldsymbol{\sigma} \cdot \mathbf{n} \right) \cdot \mathbf{s} = 0. \tag{2.1.12}$$

Now, the total stress is replaced by $\boldsymbol{\sigma} = -P\mathbf{I} + \mathbf{T}$, where $\mathbf{T}$ is the excess stress and $\mathbf{I}$ is the identity matrix. So, equation (2.1.12) becomes

$$\left[\left(-P\mathbf{I} + \mathbf{T} \right) \cdot \mathbf{n} \right] \cdot \mathbf{s} = 0. \tag{2.1.13}$$

The scalar product of the identity matrix and the unit normal vector to the free surface is equal to the unit normal vector at the free surface. In other words, $\mathbf{I} \cdot \mathbf{n} = \mathbf{n}$, using this value into equation (2.1.13) leads to

$$-P \cdot \mathbf{n} \cdot \mathbf{s} + \mathbf{s} \cdot \mathbf{T} \cdot \mathbf{n} = 0. \tag{2.1.14}$$

The first part of equation (2.1.14) is zero, as there is a scalar product between the unit normal and unit tangent vector to the free surface (they remain perpendicular to each other). In other words, $\mathbf{n} \cdot \mathbf{s} = 0$. Using this value into equation (2.1.14) reduces to

$$\mathbf{s} \cdot \mathbf{T} \cdot \mathbf{n} = 0. \tag{2.1.15}$$

Expanding equation (2.1.15) over X, Z; the equation (2.1.15) becomes,

$$s_X n_X T_{XX} + \left(s_X n_Z + s_Z n_X \right) T_{XZ} + s_Z n_Z T_{ZZ} = 0.$$

Inserting the components of the unit normal and the unit tangent vector (from equations 2.1.6-2.1.7) in X and Z direction leads to

$$T_{XZ} + \frac{H_X}{1 - H_X{}^2} \left(T_{ZZ} - T_{XX} \right) = 0. \tag{2.1.16}$$

Similarly, the traction at the free surface in the normal direction is found by taking the scalar product of the traction vector with the unit normal vector to the free surface. Using equation (2.1.8), the scalar product of the traction vector with the unit normal vector at the free surface gives

$$\mathbf{t} \cdot \mathbf{n} = -\gamma \kappa \mathbf{n} \cdot \mathbf{n}, \tag{2.1.17}$$

where $\mathbf{t}$ is the traction vector at the free surface and it is substituted by the scalar product of the total stress $\left(\boldsymbol{\sigma} \right)$ and the unit normal $\left(\mathbf{n} \right)$ vector at the free surface, $\mathbf{t} = \boldsymbol{\sigma} \cdot \mathbf{n}$. It is known that the scalar product of the two unit normal vector is one (as they remain at zero degree angle to each other), $\mathbf{n} \cdot \mathbf{n} = 1$, using these value into equation (2.1.17) leads to

$$(\boldsymbol{\sigma} \cdot \mathbf{n}) \cdot \mathbf{n} = -\gamma \kappa. \tag{2.1.18}$$

Now, the total stress is replaced by, $\boldsymbol{\sigma} = -P\mathbf{I} + \mathbf{T},$ where $\mathbf{T}$ is the excess stress and $\mathbf{I}$ is the identity matrix. Inserting this expression into equation (2.1.18), equation (2.1.18) reduces to, $\left[(-P\mathbf{I} + \mathbf{T}) \cdot \mathbf{n} \right] \cdot \mathbf{n} = -\gamma \kappa.$ \hfill (2.1.19)

As it is known, $\mathbf{I} \cdot \mathbf{n} = \mathbf{n},$ inserting this value into equation (2.1.19) leads to

$$-P \cdot \mathbf{n} \cdot \mathbf{n} + \mathbf{n} \cdot \mathbf{T} \cdot \mathbf{n} = -\gamma \kappa. \tag{2.1.20}$$

There is a scalar product between the two unit normal vectors to the free surface in equation (2.1.20) and the value is one. In other words, $\mathbf{n} \cdot \mathbf{n} = 1.$ Using this value into equation (2.1.20) reduces to

$$P - \mathbf{n} \cdot \mathbf{T} \cdot \mathbf{n} = \gamma \kappa. \tag{2.1.21}$$

Expanding equation (2.1.21) over X, Z; equation (2.1.21) becomes,

$$P - n_X{}^2 T_{XX} - 2 n_X n_Z T_{XZ} - n_Z{}^2 T_{ZZ} = \gamma \kappa.$$

Inserting the components of the unit normal vector from equation (2.1.6) in X and Z direction and using the expression $\kappa = \dfrac{1}{R}$ leads to

$$P + H_X T_{XZ} - T_{ZZ} = \frac{\gamma}{R}. \tag{2.1.22}$$

The kinematic boundary condition describes the flow velocity in the transverse direction, which is equal to the change of surface height with time. It relates the motion of the free interface to the fluid velocities at the free surface.

$$W_H = \frac{dH}{dT} = H_T + UH_X. \qquad\qquad (2.1.23)$$

In principle, equations (2.1.3-2.1.5) can be solved subjected to the boundary conditions (2.1.22-2.1.23). However, given the small depth of shallow water flow, the governing equations are simplified further and converted to boundary-layer equations for shallow water flow, which is described in the next section.

2.2 Boundary-layer equations for shallow water flow

In this section, as the depth of shallow water flow is very small, using the suitable scaling; equations (2.1.3-2.1.5) are simplified further and converted to boundary-layer equations for shallow water flow. The layout of shallow water flow is schematically depicted in figure (2.1) in the (X, Z) plane. The X axis corresponds to the horizontal (streamwise) direction and the Z axis is chosen in the vertical (transverse) direction.

The water height in the shallow pond is denoted by $Z = H(X,T)$. For this study, the emphasis will be on the wind induced flow in shallow pond. The streamwise and transverse length scales are chosen to be the length of the pond (L) and the depth of water (D) respectively. There are mainly four main dimensionless parameters. These are the Aspect ratio (ε), the Reynolds number (Re_D), the Capillary number (Ca) and the Weber number (We). Explicitly written, these take the following form:

$$\varepsilon = \frac{D}{L}, \qquad Re_D = \frac{\rho U_0 D}{\mu}, \qquad Ca = \frac{\mu U_0}{\gamma}, \qquad We = \frac{\varepsilon^3}{Ca}, \qquad (2.2.1)$$

where U_0 is the wind velocity measured at a reference height (usually 10 meter) over the shallow pond, γ is the surface tension and the Reynolds number is based on the characteristics length scale (D).

In this study, the ratio of the water depth to the length of pond is too small $(\varepsilon \ll 1)$, which is named as the aspect ratio. Thus, ε is taken as the perturbation parameter to reduce the problem to the boundary-layer type. The scaling of the position co-ordinates, velocity, pressure, time and stress components are obvious, leading to (where in scaling of time, σ is used known as wind frequency)

$$u = \frac{U}{U_0}, \qquad w = \frac{W}{\frac{D}{L}U_0}, \qquad t = \sigma T, \qquad x = \frac{X}{L},$$

$$z = \frac{Z}{D}, \qquad p = \frac{P}{\left(\mu \frac{U_0}{\varepsilon^2 L}\right)}, \qquad h = \frac{H}{D}, \qquad \tau_{xx} = \frac{T_{xx}}{\frac{\mu U_0}{L}},$$

$$\tau_{zz} = \frac{T_{zz}}{\mu \frac{U_0}{L}}, \qquad \tau_{xz} = \tau_{zx} = \frac{T_{XZ}}{\mu \frac{U_0}{D}} = \frac{T_{ZX}}{\mu \frac{U_0}{D}}. \qquad (2.2.2)$$
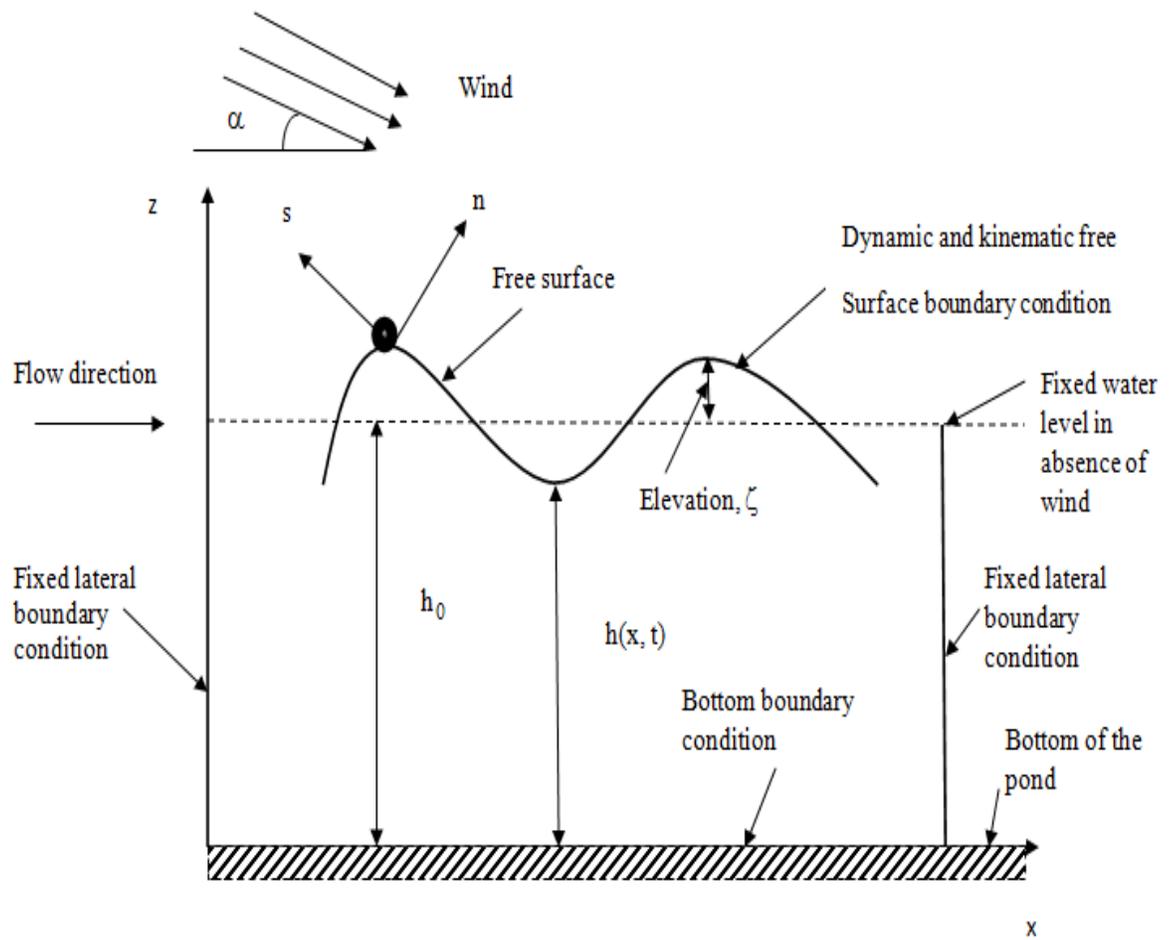
Fig2.2 Schematic of the flow domain showing the relation between ζ (elevation), h_0 (the depth of water when there is no wind action) and h (the depth of water when wind is acting over the pond)

Figure (2.2) illustrates the flow domain in non-dimensional form, where h_0 represent the fixed water level without the wind action and h represent the depth of water when wind is acting over the flow domain. Three types of boundary conditions (bottom boundary condition, lateral boundary condition and free surface boundary condition) are used to solve the problem. Wind creates drag on the water surface which is termed as the wind boundary condition on the water surface. Though in most of the existing studies wind acts parallel to the length of the pond but in our formulation we have taken that wind acts at an angle α to the positive x-axis of the flow domain. In this figure (2.2), x and z represent the horizontal (streamwise) and the vertical (transverse) direction of the flow domain, where D and L are the characteristics vertical and horizontal length scale of the shallow pond respectively. Upon introducing dimensionless variables from equation (2.2.2) into equations (2.1.3-2.1.5), and ignoring the terms of $O\left(\varepsilon^2\right)$ or higher, the relevant equations for the problem reduce to non-dimensional form as

$$\frac{\partial u}{\partial x} + \frac{\partial w}{\partial z} = 0, \tag{2.2.3}$$

$$\varepsilon \operatorname{Re}_D \left(r \frac{\partial u}{\partial t} + u \frac{\partial u}{\partial x} + w \frac{\partial u}{\partial z} \right) = -\frac{\partial p}{\partial x} + \frac{\partial \tau_{zx}}{\partial z}, \tag{2.2.4}$$

$$\frac{\partial p}{\partial z} = -G, \tag{2.2.5}$$

where in the governing equations, $r = \dfrac{\sigma L}{U_0}$ is the dimensionless frequency of the wind wave and σ is the frequency of the wind cycle over the flow domain. $G = \dfrac{\varepsilon D^2 \rho g}{\mu U_0}$ is the

Gravity number which is the ratio of the Reynolds number to the Froude number.

$$G = \frac{Re_D}{Fr}$$

The reduced conservation equations are derived using the suitable scaling, where the terms of O (ε^2) or higher are excluded from the problem formulation. As it is known that the boundary-layer flow is a shear dominated flow, so after scaling, it is found that the normal stresses are negligible as they are of O (ε^2).

The scaling method is applied to the dynamic boundary condition (equation 2.1.16) in the tangential direction. The boundary condition is expressed in non-dimensional form as

$$\tau_{xz} + \frac{\varepsilon^2 h_x}{1 - (\varepsilon h_x)^2} (\tau_{zz} - \tau_{xx}) = 0. \tag{2.2.6}$$

Ignoring the terms of $O\left(\varepsilon^2\right)$ in equation (2.2.6), results in the vanishing of the shear stress at the free surface as

$$\tau_{xz} = 0. \tag{2.2.7}$$

The radius of curvature (equation 2.1.9) in dimensional form is expressed as

$$\kappa = \frac{1}{R} = -\frac{H_{XX}}{\left(1 + H_X^2\right)^{\frac{3}{2}}}, \tag{2.2.8}$$

where (R) is the radius of curvature of the free surface and it is non-dimensionalized (r_c)

using the horizontal length scale (L). Using the scaling $r_c = \dfrac{R}{L}$, the radius of curvature

(equation 2.2.8) is expressed in non-dimensional form as

$$\kappa = \frac{1}{Lr_c} = -\frac{\dfrac{D}{L^2}h_x}{\left(1+\left(\dfrac{D}{L}h_x\right)^2\right)^{\frac{3}{2}}}.$$ (2.2.9)

Inserting the expression $\dfrac{D}{L} = \varepsilon$ as the aspect ratio, expression (2.2.9) becomes

$$\kappa = \frac{1}{Lr_c} = -\frac{\dfrac{\varepsilon}{L}h_x}{\left(1+\varepsilon^2 h_{xx}{}^2\right)^{\frac{3}{2}}}.$$ (2.2.10)

Ignoring the term of $O\left(\varepsilon^2\right)$ in expression (2.2.10), expression (2.2.10) reduces to

$$\kappa = \frac{1}{Lr_c} = -\frac{\varepsilon}{L}h_x.$$ (2.2.11)

Now, the non-dimensional dynamic boundary condition in the normal direction is found,

when the scaling is applied to equation (2.1.22). The expressions from equations (2.2.7

and 2.2.11) are inserted into equation (2.1.22) leads to

$$p\left(\frac{\mu U_0}{\epsilon^2 L}\right) - \frac{\mu U_0}{L}\tau_{zz} = -\frac{\gamma \epsilon h_x}{L}.$$ (2.2.12)

Inserting the expression of capillary number from expression (2.2.1) into equation (2.2.12), equation (2.2.12) reduces to

$$\left(\frac{p}{\epsilon^2} - \tau_{zz}\right) = -\frac{\epsilon h_x}{Ca}.$$ (2.2.13)

So, the expression for the pressure at the free surface becomes

$$p(x, z = h, t) = \epsilon^2 \tau_{zz} - \frac{\epsilon^3 h_x}{Ca}.$$ (2.2.14)

This is the dynamic boundary condition in the normal direction at the free surface. The expression for the pressure is found by integrating equation (2.2.5) with respect to z as

$$p = -Gz + c(x, t),$$ (2.2.15)

where $c(x, t)$ is an integration constant. Now, substituting the expression of the pressure at the free surface from expression (2.2.15) leads to

$$\epsilon^2 \tau_{zz} - \frac{\epsilon^3 h_x}{Ca} = -Gh + c(x, t).$$ (2.2.16)

Now, the value of $c(x, t)$ is found as

$$c(x, t) = \epsilon^2 \tau_{zz} - \frac{\epsilon^3 h_x}{Ca} + Gh.$$ (2.2.17)

Inserting the expression of $c(x, t)$ into equation (2.2.15), the expression of the pressure becomes

$$p = G(z - h) + \varepsilon^2 \tau_{zz} - \frac{\varepsilon^3 h_x}{Ca}. \tag{2.2.18}$$

Ignoring the term of $O(\varepsilon^2)$ in equation (2.2.18), equation (2.2.18) reduces to

$$p = G(z - h) - \frac{\varepsilon^3 h_x}{Ca}. \tag{2.2.19}$$

Though in the problem formulation the terms of $O(\varepsilon^2)$ or higher is neglected, the second term in equation (2.2.19) is not neglected as it is assumed that the capillary number is too small to compensate the effect of $O(\varepsilon^3)$. Differentiating the pressure with respect to x, equation (2.2.19) gives

$$\frac{\partial p}{\partial x} = -G \frac{\partial h}{\partial x} - \frac{\varepsilon^3}{Ca} \frac{\partial}{\partial x}(h_x). \tag{2.2.20}$$

Now, h is the depth of water when wind is acting over the shallow pond and ζ is the elevation from the reference level (fixed water level, the level of water when there is no wind action over the shallow pond). So, the expression of h becomes

$$h = 1 + \zeta. \tag{2.2.21}$$

The expression for first, second derivative of h with respect to x and first derivative of h with respect to t are found as

$$\frac{\partial h}{\partial x} = \frac{\partial \zeta}{\partial x}, \frac{\partial^2 h}{\partial x^2} = \frac{\partial^2 \zeta}{\partial x^2} \text{ and } \frac{\partial h}{\partial t} = \frac{\partial \zeta}{\partial t}. \tag{2.2.22}$$

Substituting the expressions of $\dfrac{\partial h}{\partial x}$ and $\dfrac{\partial^2 h}{\partial x^2}$ into equation (2.2.20), gives the value of

the pressure derivative as

$$\frac{\partial p}{\partial x} = p_x = -G\zeta_x - \frac{\varepsilon^3}{Ca}\zeta_{xx}. \tag{2.2.23}$$

The scaling method is then applied to the kinematic boundary conditions (2.1.23), the

kinematic boundary condition at the free surface (z = h) is expressed in non-dimensional

form as

$$w_h = \frac{\sigma D \partial h}{\varepsilon U_0 \partial t} + \frac{u U_0}{\varepsilon U_0} \frac{D \partial h}{L \partial x}. \tag{2.2.24}$$

Substituting the expression of $\dfrac{D}{L} = \varepsilon$ into equation (2.2.24), equation (2.2.24) reduces to

$$w_h = \frac{\sigma L \partial h}{U_0 \partial t} + u \frac{\partial h}{\partial x}. \tag{2.2.25}$$

Introducing a new dimensionless parameter (r) into equation (2.2.25), where $r = \dfrac{\sigma L}{U_0}$ is

the dimensionless frequency of the wind wave over the shallow pond. Simplifying

equation (2.2.25) leads to

$$w_h = r h_t + u h_x. \tag{2.2.26}$$

Similarly, the kinematic boundary condition at (z = 0) is expressed in non-dimensional form as

$$w_0 = 0. \qquad\qquad (2.2.27)$$

In this section, as the depth of shallow water flow is very small, using the suitable scaling; the equations are converted to boundary-layer equations for shallow water flow. In the next section, the effects of wind and the bottom are incorporated in the governing equations which come through the wind and bottom stresses to formulate the problem.

2.3 Incorporation of the wind conditions and the bottom shear stress

In this section, the influence of the wind action and the effect of bottom are incorporated in the governing equations. The influences of the wind action and the bottom of the pond come through the wind and bottom stress terms in the boundary-layer equations for shallow water flow.

Wind boundary conditions:

When wind blows over water it exerts a shear stress on the water surface. Although the wind shear stress is usually very small in shallow or thin film flow domain but its effect, when integrated over a shallow or thin-film flow domain, can be catastrophic. Wind creates drag force on the water surface which is termed as the wind boundary condition or wind stress on the water surface. The water surface layer is accelerated in the direction of the wind stress. Once this surface layer of water has attained a velocity, a stress is exerted on the adjacent layer. The wind stress can be estimated in a shallow pond using any one of the several formulas found in the literature.

(Wu's equation as presented in the RMA2 Users Guide (U.S. Army Corps of Engineers-Waterways Experiment Station, 1996) and Van Dorn's equation (Dean and Dalrymple, 1991)).

Oscillatory wind is the main driving force to cause resuspension in a shallow tailings pond. The wind stress is directed at an angle (α) to the positive X-axis of the flow domain. Matthews et al. (Appl. Math. Modelling, 1996) have used $\alpha = 0$ to express the periodic wind forcing acts in the X direction over the flow domain. So, using $\alpha = 0$ in the wind stress expression by (Mclnerney, Teubner and Noye 2010) resembles the wind stress expression by Matthews et al.

There are several expressions available in the literature by which wind stress can be expreesed.Wind stress can be expressed by Coastal and Ocean Engineering (Fenton 2010) as,

$$\tau = \rho C_d U_0{}^2,$$

where C_d is the drag coefficient $C_d = .0075 + .000067 U_0$, in which U_0 is the wind speed at a height of 10m, and ρ is the density of air. The actual speed of the ocean current is a small fraction of the wind speed, roughly 3-5%.

In the modeling of the wind-driven circulation in a tailings pond, it is necessary to know the horizontal shear stress imposed as a boundary condition at the surface of the pond. This stress is caused by the interaction of the turbulent air and water. The relation of this stress to the wind speed is very difficult to determine from theoretical considerations and its value is usually based on the semi empirical formulas and on

observations. The formula or the expression for wind stress given by (Lick 1976) is as follows,

$$\tau = \rho C_d U_0^{n-1} U_0,$$

where C_d is a drag coefficient, ρ is the density of the air, U_0 is the wind velocity measured at 10 m height above the water surface, and n is an empirically determined exponent not necessarily integer. Wilson (1960) has analyzed the data from many different sources and has given a best fit to the data. For U_0 in units of cm/sec, Pa in units of gm/cm^3, and τ in units of $dynes/cm^2$, Wilson suggests a value of n=2 and C_d =0.00237 for strong winds and 0.00166 for light winds. From a comparison of field data and results of numerical models, Simons (1974) suggests values of n=2 and C_d=0.003.

Though in most of the existing studies wind acts parallel over the length of the shallow tailings pond but we have assumed that the wind acts at an angle α to the positive X-axis of the flow domain and used the expression of the wind stress by (Mclnerney, Teubner and Noye 2010) in the momentum equation. In the X-momentum equation (2.1.4), $T_{ZX}|_{Z=H} = T_S = T_0 \cos\alpha \cos(\sigma T)$ is the wind stress with magnitude T_0 and frequency σ (which is the frequency of the wind cycle). $T_{ZX}|_{Z=H} = T_S$ is simply a representation of wind stress with

- Maximum magnitude of $T_0 = \rho C_d U_0^2$,

- Wind oscillates over time T, cos (σ T) varies between -1 and 1.

- The wind is directed at an angle of alpha (α) to the X-axis. (The X-component of the wind corresponds to $\cos\alpha$).

- The wind stress is not meant to be realistic. The simplicity of this equation enabled us to produce the analytic solution. We have tried to use this expression as a different approach to express the wind stress working over the flow domain. By setting $\alpha = 0$ and ignoring time dependency it resembles the traditional or realistic wind force acts parallel over the flow domain.

- The wind stress is assumed to be periodic with time to observe the effect of the flow field under the periodic wind condition.

- The wind is taken at an angle with the X-axis of the flow domain. But in most of the existing studies it is found that, wind acts parallel over the shallow flow domain. So using wind at an angle (α) can sometimes limits the use of the present wind stress expression in real life problems. Now the wind stress expression will be incorporated in the X-momentum equation (2.1.4) as,

$$T_{ZX}\big|_{Z=h} = T_s = T_0 (\cos\alpha)\cos(\sigma T), \qquad (2.3.1)$$

where $T_0 = \rho C_d U_0^{\,2}$ is the magnitude of the wind stress and C_d is the wind/surface friction co-efficient. Typical value of C_d is of $O(10^{-3})$. U_0 is the wind velocity measured at a reference height over the shallow pond. After the scaling, the surface stress is expressed in non-dimensional form as

$$\tau_{zx}\big|_{z=h} = \tau_s = \frac{\rho C_d U_0^2}{\dfrac{\mu U_0}{D}}(\cos\alpha)\cos(t) = C_d \operatorname{Re}_D(\cos\alpha)\cos(t). \qquad (2.3.2)$$

Incorporation of bottom stress:

Similarly, in the X-momentum equation (2.1.4) $T_{ZX}\big|_{Z=0} = T_b$ is the bottom stress in dimensional form. It is commonly expressed empirically using the quadratic law, where C_b is the bottom friction co-efficient. Typical value of C_b is of $O(10^{-3})$. The bottom stress (Tsanis & Saied 2005) is expressed in dimensional form as

$$T_{ZX}\big|_{Z=0} = T_b = \rho C_b U |U|, \qquad (2.3.3)$$

where ρ is the density and U is the flow velocity of water in dimensional form. The bottom stress after the scaling is expressed in non-dimensional form as

$$\tau_{zx}\big|_{z=0} = \tau_b = \frac{\rho C_b u^2 U_0 |U_0|}{\dfrac{\mu U_0}{D}} = C_b \operatorname{Re}_D u^2. \qquad (2.3.4)$$

The depth integrated velocity (flow rate) q is expressed as

$$q = \int_0^h u \, dz. \qquad (2.3.5)$$

From shallow water assumptions, as u is independent of z, equation (2.3.5) reduces to

$$q = u \int_0^h dz = uh.$$ (2.3.6)

So, the expression of the bottom stress (equation 2.3.4) in terms of depth integrated velocity (flow rate) is expressed as

$$\tau_{zx}\big|_{z=0} = \tau_b = C_b \, Re_D \, u^2 = C_b \, Re_D \, \frac{q^2}{h^2}.$$ (2.3.7)

Now, integrating equation (2.2.3) over the depth of water (between 0 to h), the continuity equation becomes $\int_0^h \left(\frac{\partial u}{\partial x} + \frac{\partial w}{\partial z} \right) dz = 0.$ (2.3.8)

After integrating equation (2.3.8) with respect to z, equation (2.3.8) reduces to

$$\int_0^h \left(\frac{\partial u}{\partial x} \right) dz + w_h - w_0 = 0.$$ (2.3.9)

Now, using the Leibniz rule, the value of the term $\int_0^h \left(\frac{\partial u}{\partial x} \right) dz$ is determined as

$$\int_0^h \left(\frac{\partial u}{\partial x} \right) dz = \frac{\partial}{\partial x} \int_0^h u\, dz - u \frac{\partial h}{\partial x}.$$ (2.3.10)

As u is independent upon z, the following expression is found as

$$\frac{\partial}{\partial x} \int_0^h u\, dz = \frac{\partial}{\partial x} u \int_0^h dz = \frac{\partial}{\partial x}(uh).$$ (2.3.11)

Inserting the expression of $\dfrac{\partial}{\partial x}\displaystyle\int_0^h u\,dz$ from equation (2.3.11) into equation (2.3.10) leads

to

$$\int_0^h \left(\frac{\partial u}{\partial x}\right)dz = \frac{\partial}{\partial x}(uh) - u\frac{\partial h}{\partial x}. \qquad (2.3.12)$$

The values of the terms $\displaystyle\int_0^h \left(\dfrac{\partial u}{\partial x}\right)dz$, $\left(w_h, w_0\right)$ found from equations (2.3.12, 2.2.26-2.2.27)

are inserted into equation (2.3.9) gives

$$\frac{\partial}{\partial x}(uh) - uh_x + rh_t + uh_x = rh_t + \frac{\partial}{\partial x}(uh) = 0. \qquad (2.3.13)$$

The value of the depth integrated velocity (q) from equation (2.3.6) is inserted into

equation (2.3.13), and using the expression of $\dfrac{\partial h}{\partial t}$ from equation (2.2.22) into equation

(2.3.13) reduces to

$$r\frac{\partial \zeta}{\partial t} + \frac{\partial q}{\partial x} = 0. \qquad (2.3.14)$$

Now, equation (2.2.4) is integrated over the depth of water between 0 to h. From shallow

water approximation it is known that u is independent upon z, setting $\dfrac{\partial u}{\partial z} = 0$ into

equation (2.2.4), equation (2.2.4) reduces to

$$\varepsilon\,Re_D\left(rhu_t + uhu_x\right) = -\frac{\partial p}{\partial x}h + \tau_{zx}\big|_{z=h} - \tau_{zx}\big|_{z=0}. \qquad (2.3.15)$$

Substituting the expressions of pressure gradient, wind and bottom stress from equations (2.2.23) and (2.3.2-2.3.4) into equation (2.3.15) yields

$$\varepsilon \, Re_D \left(rhu_t + uhu_x \right) = Gh \frac{\partial \zeta}{\partial x} + Weh \frac{\partial^2 \zeta}{\partial x^2} + C_d \, Re_D \left(\cos \alpha \right) \cos t - C_b \, Re_D \frac{q^2}{h^2},$$

(2.3.16)

where $We = \dfrac{\varepsilon^3}{Ca}$ is the Weber number and Ca is the capillary number. Dividing the both side of equation (2.3.16) with $\varepsilon \, Re_D$ results in

$$\left(rhu_t + uhu_x \right) = \frac{1}{\varepsilon \, Re_D} \left(Gh \frac{\partial \zeta}{\partial x} + Weh \frac{\partial^2 \zeta}{\partial x^2} + C_d \, Re_D \left(\cos \alpha \right) \cos t - C_b \, Re_D \frac{q^2}{h^2} \right).$$

(2.3.17)

From equation (2.3.13) it can be shown that

$$rh_t + \frac{\partial}{\partial x} \left(uh \right) = rh_t + uh_x + hu_x = 0. \tag{2.3.18}$$

Multiplying equation (2.3.18) with u gives

$$urh_t + u \left(uh_x + hu_x \right) = 0. \tag{2.3.19}$$

Adding equations (2.3.17 and 2.3.19) results in

$$urh_t + rhu_t + 2huu_x + u^2 h_x = \frac{1}{\varepsilon \, Re_D} \left(Gh \frac{\partial \zeta}{\partial x} + Weh \frac{\partial^2 \zeta}{\partial x^2} + C_d \, Re_D \left(\cos \alpha \right) \cos t - C_b \, Re_D \frac{q^2}{h^2} \right).$$

(2.3.20)

Substituting the expressions of $\frac{\partial}{\partial t}(ruh) = ruh_t + rhu_t$ and $\frac{\partial}{\partial x}(u^2 h) = u^2 h_x + 2huu_x$ into

equation (2.3.20) gives

$$\frac{\partial}{\partial t}(ruh) + \frac{\partial}{\partial x}(u^2 h) = \frac{1}{\varepsilon \operatorname{Re}_D}\left(Gh\frac{\partial \zeta}{\partial x} + Weh\frac{\partial^2 \zeta}{\partial x^2} + C_d \operatorname{Re}_D (\cos \alpha)\cos t - C_b \operatorname{Re}_D \frac{q^2}{h^2}\right).$$

(2.3.21)

Inserting the expression of depth integrated velocity (flow rate) from equation (2.3.6) into

equation (2.3.21) leads to

$$r\frac{\partial q}{\partial t} + \frac{\partial}{\partial x}\left(\frac{q^2}{h}\right) = \frac{1}{\varepsilon \operatorname{Re}_D}\left(Gh\frac{\partial \zeta}{\partial x} + Weh\frac{\partial^2 \zeta}{\partial x^2} + C_d \operatorname{Re}_D (\cos \alpha)\cos t - C_b \operatorname{Re}_D \frac{q^2}{h^2}\right).$$

(2.3.22)

The boundary conditions at the two lateral boundaries of the shallow pond are given by

$$\left.\begin{array}{l} q(x=0,t) = q(x=1,t) = 0 \\ \zeta(x=0,t) = 0 \end{array}\right\},$$

(2.3.23)

where the first two boundary conditions are the no-penetration boundary condition at the

two lateral boundaries of the shallow pond and the third boundary condition demonstrates

the elevation is zero for any time at zero position of the x co-ordinate. In this section, the

influences of wind action and the effect of bottom are incorporated in the governing

equations. In the next section, the equations (2.3.14 and 2.3.22) are solved using a small

perturbation approach subjected to the boundary conditions (2.3.23).

2.4. Solution Procedure

In this section, the equations (2.3.14 and 2.3.22) are solved using a small perturbation approach subjected to the boundary conditions (2.3.23). A third order ODE is solved to find the three roots of the ODE. Using these three roots, the expression of the elevation is found by solving the governing equations. With the help of the expression of the elevation, the expression of the flow velocity is found using the continuity equation. The expression for the bottom stress is found using the empirical relation (2.3.4), where the bottom stress depends on the flow velocity. The expressions of the flow field (elevation, flow velocity and bottom shear stress) are found as the solution of the governing equations (2.3.14 and 2.3.22). In the present study, the surface tension component is not neglected and the change in the flow behavior due to surface tension is also studied.

A small perturbation approach is used to solve equations (2.3.14 and 2.3.22), where it is assumed that the elevation is an order of magnitude smaller than the depth of water. Solutions of equations (2.3.14-2.3.22) are of the following form

$$\zeta = \sum_{n=1} \varepsilon^n \zeta_n \approx \varepsilon^1 \zeta_1, \tag{2.4.1a}$$

$$q = \sum_{n=1} \varepsilon^n q_n \approx \varepsilon^1 q_1, \tag{2.4.1b}$$

where ε is the small perturbation parameter and ζ_1, q_1 are the first order elevation and flow rate (depth integrated velocity) respectively in the problem formulation. Now, expanding $1/h$, using small perturbation approach up to $O(\varepsilon)$ leads to

$$\frac{1}{h} = \frac{1}{1+\zeta} = \frac{1}{1+\varepsilon\zeta_1} = 1\left(1+\varepsilon\frac{\zeta_1}{1}\right)^{-1} = 1\left(1-\varepsilon\zeta_1 + \left(\varepsilon\zeta_1\right)^2 - \left(\varepsilon\zeta_1\right)^3 + \ldots\ldots\ldots\ldots\right) = 1\left(1-O(\varepsilon)\right).$$
(2.4.2)

Now, using equations (2.4.1a and 2.4.1b) to formulate the problem for first order solution, equation (2.3.14) yields

$$r\frac{\partial\zeta_1}{\partial t} = -\frac{\partial q_1}{\partial x}.$$
(2.4.3)

It is known from equation (2.4.1b), that the depth integrated velocity is of $O(\varepsilon)$ so, the bottom stress (equation 2.3.10) having $O\left(\varepsilon^2\right)$ is neglected for first order solution (as in problem formulation the terms of $O\left(\varepsilon^2\right)$ or higher are neglected). Therefore, for first order solution equation (2.3.22) becomes

$$r\frac{\partial q_1}{\partial t} = \frac{1}{\varepsilon \text{Re}_D}\left(Gh\frac{\partial\zeta_1}{\partial x} + Weh\frac{\partial^2\zeta_1}{\partial x^2} + \frac{C_d \text{Re}_D\left(\cos\alpha\right)\cos t}{\varepsilon}\right).$$
(2.4.4)

Using equation (2.4.1b) to insert the expression of h, and omitting the terms of $O(\varepsilon)$ yields the first order solution as

$$r\frac{\partial q_1}{\partial t} = \frac{1}{\varepsilon \text{Re}_D}\left(G\frac{\partial\zeta_1}{\partial x} + We\frac{\partial^2\zeta_1}{\partial x^2} + \frac{C_d \text{Re}_D\left(\cos\alpha\right)\cos t}{\varepsilon}\right).$$
(2.4.5)

Applying the boundary conditions (2.3.26) and neglecting the terms of $O(\varepsilon)$, yields the boundary conditions for the first order solution at the two lateral boundaries of the shallow pond as

$$q_1\left(x=0,t\right)=q_1\left(x=1,t\right)=0, \tag{2.4.6}$$

$$\zeta_1\left(x=0,t\right)=0. \tag{2.4.7}$$

Now, equation (2.4.5) is differentiated with respect to x, leads to

$$r\frac{\partial}{\partial x}\left(\frac{\partial q_1}{\partial t}\right)=\frac{1}{\varepsilon\,\mathrm{Re}_D}\left(G\frac{\partial^2\zeta_1}{\partial x^2}+\mathrm{We}\frac{\partial^3\zeta_1}{\partial x^3}\right). \tag{2.4.8}$$

Inserting the expression of $\dfrac{\partial q_1}{\partial x}$ from equation (2.4.1.3) into equation (2.4.8) gives

$$r\frac{\partial}{\partial t}\left(-r\frac{\partial\zeta_1}{\partial t}\right)=\frac{1}{\varepsilon\,\mathrm{Re}_D}\left(G\frac{\partial^2\zeta_1}{\partial x^2}+\mathrm{We}\frac{\partial^3\zeta_1}{\partial x^3}\right). \tag{2.4.9}$$

Dividing equation (2.4.9) with the Weber number (We) leads to

$$\frac{\partial^3\zeta_1}{\partial x^3}-\frac{G}{\mathrm{We}}\frac{\partial^2\zeta_1}{\partial x^2}-\frac{\varepsilon r^2\,\mathrm{Re}_D}{\mathrm{We}}\frac{\partial^2\zeta_1}{\partial t^2}=0. \tag{2.4.10}$$

Introducing two new parameters in equation (2.4.10) as

$$\frac{G}{\mathrm{We}}=a,\qquad\qquad\frac{\varepsilon r^2\,\mathrm{Re}_D}{\mathrm{We}}=b. \tag{2.4.11}$$

Inserting these new parameters into equation (2.4.11) leads to

$$\frac{\partial^3\zeta_1}{\partial x^3}-a\frac{\partial^2\zeta_1}{\partial x^2}-b\frac{\partial^2\zeta_1}{\partial t^2}=0. \tag{2.4.12}$$

The boundary conditions are also changed and expressed in terms of first order elevation.

Using the boundary condition (2.4.6) for first order solution, it is found that $\dfrac{\partial q_1}{\partial t} = 0$. So,

substituting this expression into equation (2.4.5) results

$$G \frac{\partial \zeta_1}{\partial x} - We \frac{\partial^2 \zeta_1}{\partial x^2} = \frac{C_d \, Re_D (\cos \alpha) \cos t}{\varepsilon}. \qquad (2.4.13)$$

Dividing equation (2.4.13) with the Weber number (We) and substituting $\dfrac{G}{We} = a$

reduces to

$$\frac{\partial^2 \zeta_1}{\partial x^2} - a \frac{\partial \zeta_1}{\partial x} = - \frac{C_d \, Re_D (\cos \alpha) \cos t}{\varepsilon We}. \qquad (2.4.14)$$

Now, the boundary conditions are expressed in terms of first order elevation as

$$\left(\frac{\partial^2 \zeta_1}{\partial x^2} - a \frac{\partial \zeta_1}{\partial x} \right) \Bigg|_{x=0} = \left(\frac{\partial^2 \zeta_1}{\partial x^2} - \frac{\partial \zeta_1}{\partial x} \right) \Bigg|_{x=1} = - \frac{C_d \, Re_D (\cos \alpha) \cos t}{\varepsilon We}. \qquad (2.4.15)$$

The third boundary condition is found from equation (2.4.7) as

$$\zeta_1 \big|_{x=0} = 0. \qquad (2.4.16)$$

The most general form of ζ_1 as a solution of equation (2.4.12) is expressed as

$$\zeta_1 = Z(x) \cos t. \qquad (2.4.17)$$

Now, taking the second derivative of ζ_1 with respect to x, t and the first and third derivative of ζ_1 with respect to x gives

$$\frac{\partial \zeta_1}{\partial x} = \frac{dZ}{dx}\cos t, \qquad\qquad \frac{\partial^2 \zeta_1}{\partial x^2} = \frac{d^2 Z}{dx^2}\cos t. \qquad\qquad (2.4.18)$$

$$\frac{\partial^3 \zeta_1}{\partial x^3} = \frac{d^3 Z}{dx^3}\cos t, \qquad\qquad \frac{\partial^2 \zeta_1}{\partial t^2} = Z(-\cos t). \qquad\qquad (2.4.19)$$

Inserting the expressions from equations (2.4.18-2.4.19) into equation (2.4.12), to express equation (2.4.12) in terms of Z leads to,

$$\left(\frac{d^3 Z}{dx^3} - a\frac{d^2 Z}{dx^2} - bZ\right)\cos t = 0. \qquad\qquad (2.4.20)$$

From equation (2.4.20), one ODE is found in terms of Z, namely

$$\frac{d^3 Z}{dx^3} - a\frac{d^2 Z}{dx^2} - bZ = Z''' - aZ'' - bZ = 0. \qquad\qquad (2.4.21)$$

Clearly, $Z = e^{mx}$ is a solution of equation (2.4.21), so equation (2.4.21) in terms of m becomes

$$m^3 - am^2 - b = 0. \qquad\qquad (2.4.22)$$

Solving equation (2.4.22), three roots (one is real and two are complex conjugate) are determined as

$$m_1 = \text{real}$$
$$m_2 = p + iq \Big\}.$$
$$m_3 = p - iq$$

(2.4.23)

Solution of equation (2.4.21) takes the following form

$$Z = Ae^{m_1 x} + Be^{m_2 x} + Ce^{m_3 x}.$$

(2.4.24)

Substituting the values of m_2, m_3 in expression of Z, equation (2.4.24) reduces to

$$Z = Ae^{m_1 x} + Be^{(p-iq)x} + Ce^{(p+iq)x}.$$

(2.4.25)

Using de Moivre's formula $\left(e^{ix} = \cos x + i \sin x \right)$, equation (2.4.25) can be written as

$$Z = Ae^{m_1 x} + Be^{px} \left(\cos qx - i \sin qx \right) + Ce^{px} \left(\cos qx + i \sin qx \right).$$

(2.4.26)

The constants B and C are divided into two parts; the real part $\left(B_r, C_r \right)$ and the imaginary part $\left(B_i, C_i \right)$ are inserted into equation (2.4.26) as

$$Z = Ae^{m_1 x} + B_r e^{px} \left(\cos qx - i \sin qx \right) + iB_i e^{px} \left(\cos qx - i \sin qx \right)$$
$$+ C_r e^{px} \left(\cos qx + i \sin qx \right) + iC_i e^{px} \left(\cos qx + i \sin qx \right).$$

(2.4.27)

Substituting $B_r + iB_i + C_r + iC_i = B'$ and $iB_r + B_i + iC_r - C_i = C'$, and dropping the prime, equation (2.4.27) reduces to

$$Z = Ae^{m_1 x} + Be^{px} \cos qx + Ce^{px} \sin qx.$$

(2.4.28)

To find the values of the constants (A, B and C) in equation (2.4.28), three boundary conditions are needed in terms of Z. Now, the boundary conditions expressed in terms of first order elevation (2.4.14) are expressed in terms of Z as

$$\left.\left(\frac{d^2Z}{dx^2} - a\frac{dZ}{dx}\right)\right|_{x=0}\cos t = \left.(Z'' - aZ')\right|_{x=0}\cos t = -\frac{C_d \, Re_D \, (\cos\alpha)\cos t}{\varepsilon We}, \qquad (2.4.29)$$

And

$$\left.\left(\frac{d^2Z}{dx^2} - a\frac{dZ}{dx}\right)\right|_{x=1}\cos t = \left.(Z'' - aZ')\right|_{x=1}\cos t = -\frac{C_d \, Re_D \, (\cos\alpha)\cos t}{\varepsilon We}. \qquad (2.4.30)$$

Equating the coefficient of cost of equations (2.4.29 and 2.4.30) one should then have

$$\left.\left(\frac{d^2Z}{dx^2} - a\frac{dZ}{dx}\right)\right|_{x=0} = \left.(Z'' - aZ')\right|_{x=0} = -\frac{C_d \, Re_D \, (\cos\alpha)}{\varepsilon We} = c, \qquad (2.4.31)$$

$$\left.\left(\frac{d^2Z}{dx^2} - a\frac{dZ}{dx}\right)\right|_{x=1} = \left.(Z'' - aZ')\right|_{x=1} = -\frac{C_d \, Re_D \, (\cos\alpha)}{\varepsilon We} = c, \qquad (2.4.32)$$

where $-\dfrac{C_d \, Re_D \, (\cos\alpha)}{\varepsilon We} = c.$

Using the boundary condition (2.4.15), the third boundary condition is expressed in terms of Z. As $\left.\zeta_1\right|_{x=0} = Z(x)\cos t = 0$, therefore, Z should be zero at x = 0 as the third boundary condition of the flow domain, expressed as

$$Z\big|_{x=0} = 0. \tag{2.4.33}$$

Now, with the help of equation (2.4.27), the first and second derivative of Z with respect to x are found as

$$\frac{dZ}{dx} = m_1 A e^{m_1 x} + B e^{px}\left(p\cos qx - q\sin qx\right) + C e^{px}\left(p\sin qx + q\cos qx\right). \tag{2.4.34}$$

$$\frac{d^2 Z}{dx^2} = m_1{}^2 A e^{m_1 x} + B e^{px}\left(p^2\cos qx - 2pq\sin qx - q^2\cos qx\right) \tag{2.4.35}$$
$$+ C e^{px}\left(p^2\sin qx + 2pq\cos qx - q^2\sin qx\right).$$

Inserting the values of x = 0, 1 into equation (2.4.34), equation (2.4.34) reduces to

$$\frac{dZ}{dx}\bigg|_{x=0} = m_1 A + pB + qC. \tag{2.4.36}$$

$$\frac{dZ}{dx}\bigg|_{x=1} = m_1 A e^{m_1} + B e^{p}\left(p\cos q - q\sin q\right) + C e^{p}\left(p\sin q + q\cos q\right). \tag{2.4.37}$$

Similarly, the second derivative of Z with respect to x, equation (2.4.35) at x = 0, 1 reduce to

$$\frac{d^2 Z}{dx^2}\bigg|_{x=0} = m_1{}^2 A + B\left(p^2 - q^2\right) + 2pqC. \tag{2.4.38}$$

$$\frac{d^2 Z}{dx^2}\bigg|_{x=1} = m_1{}^2 A e^{m_1} + B e^{p}\left(p^2\cos q - 2pq\sin q - q^2\cos q\right) + C e^{p}\left(p^2\sin q + 2pq\cos q - q^2\sin q\right). $$
$$\tag{2.4.39}$$

Now, substituting the expressions of $\dfrac{dZ}{dx}$ from equation (2.4.1.36) and $\dfrac{d^2Z}{dx^2}$ from equation

(2.4.38) at $x = 0$ into equation (2.4.31) reduces to

$$m_1{}^2 A + B\left(p^2 - q^2\right) + 2pqC - a\left(m_1 A + pB + qC\right) = c. \qquad (2.4.40)$$

$$\Rightarrow \left(m_1{}^2 - am_1\right)A + \left(p^2 - q^2 - ap\right)B + \left(2pq - aq\right)C = c. \qquad (2.4.41)$$

Similarly, substituting the expressions of $\dfrac{dZ}{dx}$ from equation (2.4.1.37) and $\dfrac{d^2Z}{dx^2}$ from

equation (2.4.39), at $x = 1$ into equation (2.4.32) results in

$$m_1{}^2 A e^{m_1} + B e^p \left(p^2 \cos q - 2pq \sin q - q^2 \cos q\right) + C e^p \left(p^2 \sin q + 2pq \cos q - q^2 \sin q\right)$$
$$-a\left(m_1 A e^{m_1} + B e^p \left(p \cos q - q \sin q\right) + C e^p \left(p \sin q + q \cos q\right)\right) = c.$$

$$(2.4.42)$$

$$\Rightarrow \left(m_1{}^2 e^{m_1} - am_1 e^{m_1}\right)A + \left(p^2 e^p \cos q - 2pq e^p \sin q - q^2 e^p \cos q - ap e^p \cos q + aq e^p \sin q\right)B$$
$$+ \left(p^2 e^p \sin q + 2pq e^p \cos q - q^2 e^p \sin q - ap e^p \sin q - aq e^p \cos q\right)C = c.$$
$$(2.4.43)$$

Using the boundary condition (2.4.33) into equation (2.4.28) leads to

$$0 = A + B. \qquad (2.4.44)$$

Now, a set of equations are found to determine the values of the constants (A, B and C) in equation (2.4.28). To determine the values of the constants A, B and C; three equations are found as

$$
\left.\begin{array}{l}
A+B=0 \\
\left(m_1^2 - am_1\right)A + \left(p^2 - q^2 - ap\right)B + \left(2pq - aq\right)C = c \\
\left(m_1^2 e^{m_1} - am_1 e^{m_1}\right)A + \left(p^2 e^p \cos q - 2pq e^p \sin q - q^2 e^p \cos q - ap e^p \cos q + aq e^p \sin q\right)B \\
\qquad + \left(p^2 e^p \sin q + 2pq e^p \cos q - q^2 e^p \sin q - ap e^p \sin q - aq e^p \cos q\right)C = c
\end{array}\right\}.
$$

$$(2.4.45)$$

After substituting the expression of Z into equation (2.4.16), the expression for the first order elevation is found. It is found that the first order elevation depends only on cost contribution.

$$
\zeta_1 = \left[Ae^{m_1 x} + Be^{px} \cos qx + Ce^{px} \sin qx\right] \cos t. \tag{2.4.46}
$$

Now, substituting the expression of ζ_1 into equation (2.4.1a), the expression of the elevation becomes

$$
\zeta = \varepsilon \zeta_1 = \varepsilon \left[Ae^{m_1 x} + Be^{px} \cos qx + Ce^{px} \sin qx\right] \cos t. \tag{2.4.47}
$$

Inserting the expression of the first order depth integrated velocity $\left(q_1\right)$ as $q_1 = Q_1 \sin t$ into equation (2.4.3), equation (2.4.3) leads to

$$rZ(-\sin t) = -\frac{dQ_1}{dx}(\sin t).$$

(2.4.48)

Dividing equation (2.4.48) with sint reduces to,

$$rZ = \frac{dQ_1}{dx}.$$

(2.4.49)

Integrating equation (2.4.49) with respect to x between 0 to x, the expression for Q_1 is found as,

$$Q_1 = r\int_0^x Z dx$$

$$\Rightarrow Q_1 = r\left[\frac{Ae^{m_1 x}}{m_1} + \frac{Be^{px}}{p^2+q^2}(p\cos qx + q\sin qx) + \frac{Ce^{px}}{p^2+q^2}(p\sin qx - q\cos qx) - \left(\frac{A}{m_1} + \frac{Bp-Cq}{p^2+q^2}\right)\right].$$

(2.4.50)

So, the expression for the first order depth integrated velocity becomes,

$$q_1 = Q_1 \sin t = r\sin t\left[\frac{Ae^{m_1 x}}{m_1} + \frac{Be^{px}}{p^2+q^2}(p\cos qx + q\sin qx) + \frac{Ce^{px}}{p^2+q^2}(p\sin qx - q\cos qx) - \left(\frac{A}{m_1} + \frac{Bp-Cq}{p^2+q^2}\right)\right].$$

(2.4.51)

Now, using the expression of q_1 from equation (2.4.51) into equation (2.4.1b) results the expression for the depth integrated velocity (flow rate) as

$$q = \varepsilon q_1 = \varepsilon r\sin t\left[\frac{Ae^{m_1 x}}{m_1} + \frac{Be^{px}}{p^2+q^2}(p\cos qx + q\sin qx) + \frac{Ce^{px}}{p^2+q^2}(p\sin qx - q\cos qx) - \left(\frac{A}{m_1} + \frac{Bp-Cq}{p^2+q^2}\right)\right].$$

(2.4.52)

Using the expressions ζ_1, q_1 found earlier, the calculation of the flow field is done. Flow velocity is found dividing the depth integrated velocity (q) with the depth of water (h) of the shallow pond. Substituting the expression of $q_1 = u_1 h = u_1 (1 + \varepsilon \zeta_1)$ into equation (2.4.51) reduces to

$$u_1 (1 + \varepsilon \zeta_1) = r \sin t \left[\frac{A e^{m_1 x}}{m_1} + \frac{B e^{px}}{p^2 + q^2} (p \cos qx + q \sin qx) + \frac{C e^{px}}{p^2 + q^2} (p \sin qx - q \cos qx) - \left(\frac{A}{m_1} + \frac{Bp - Cq}{p^2 + q^2} \right) \right].$$

$$(2.4.53)$$

So, the expression of the flow velocity becomes,

$$u = \varepsilon u_1 = \frac{\varepsilon r \sin t}{(1 + \varepsilon \zeta_1)} \left[\frac{A e^{m_1 x}}{m_1} + \frac{B e^{px}}{p^2 + q^2} (p \cos qx + q \sin qx) + \frac{C e^{px}}{p^2 + q^2} (p \sin qx - q \cos qx) - \left(\frac{A}{m_1} + \frac{Bp - Cq}{p^2 + q^2} \right) \right].$$

$$(2.4.54)$$

Now, the expression of the bottom stress is found from equation (2.3.7) as

$$\tau_b = C_b \, Re_D \, u^2.$$

$$(2.4.55)$$

Substituting the expression of u from equation (2.4.54) into equation (2.4.55) leads to

$$\tau_b = C_b \, Re_D \left(\frac{\varepsilon r \sin t}{(1 + \varepsilon \zeta_1)} \left[\begin{array}{c} \dfrac{A e^{m_1 x}}{m_1} + \dfrac{B e^{px}}{p^2 + q^2} (p \cos qx + q \sin qx) \\ \\ + \dfrac{C e^{px}}{p^2 + q^2} (p \sin qx - q \cos qx) - \left(\dfrac{A}{m_1} + \dfrac{Bp - Cq}{p^2 + q^2} \right) \end{array} \right] \right)^2.$$

$$(2.4.56)$$

This is the expression of the bottom stress of the flow domain. In this section, a small perturbation method is used to solve the problem and finally, the expressions for the elevation, flow velocity and bottom stress are found as the solution of the problem.

In this chapter, the problem is formulated from the conservation of mass and momentum equations. Then using the suitable scaling and order of magnitude analysis the equations are converted to boundary-layer equations. From z-momentum equation it is found that the pressure distribution is hydrostatic in the transverse direction of the flow domain, where the pressure depends only on the gravitational effect. The empirical relations for wind and bottom stresses are inserted in the momentum equation. Three types of boundary conditions (bottom boundary condition, fixed lateral boundary condition and free surface boundary condition) are used to solve the problem. The effect of surface tension comes through the pressure expression in the dynamic boundary condition at the free surface. A small perturbation method is used to solve the problem and the problem is solved for the first order solution. Finally, the expressions for elevation, flow velocity and bottom stress are found as the solution of the problem.

CHAPTER 3

INFLUENCE OF INERTIA AND SURFACE TENSION

The formulation and numerical implementation above are now used to study the shallow water flow as illustrated schematically in figure (2.2). The influences of fluid inertia, surface tension and wind direction on the flow field (elevation, flow velocity and bottom stress) are investigated in this chapter. This present study considers the effect of surface tension as well as inertia on the flow field, which is a novel approach in comparison with most of the existing studies on shallow water flow.

In the current study, three parameters, $\mathrm{Re_D}, \mathrm{We} \text{ and } \alpha$ are varied to study the flow field (elevation, flow velocity and bottom Stress). Recall that the Weber number (We) is the ratio of inertia and surface tension forces, the Reynolds number ($\mathrm{Re_D}$) is the ratio of Inertia and viscous forces and α is the direction of the wind with the x-axis acting over the flow domain. The flow field at both moderately large and small values of $\mathrm{Re_D}$, We and α are examined in this study. The effect of wind comes through the oscillatory wind stress acting over the flow domain. Although the wind is uniform with respect to position, the flow responses change periodically along the horizontal position of the flow domain under the influence of wind action.

The analysis described in this chapter is different from the existing analysis (linear wave theory) to determine the bottom shear stress, where viscous and surface tension effects are neglected, while in the present analysis it considers viscous and surface tension effects. The linear wave theory assumes the fluid to be inviscid that

means no consideration of viscosity and surface tension in the theory, which is not realistic for real life flow problems. Three parameters Re_D, We and α are varied to see the influences of the surface tension, inertia and wind direction on the flow field. The influences of these parameters Re_D, We, and α are discussed in this section.
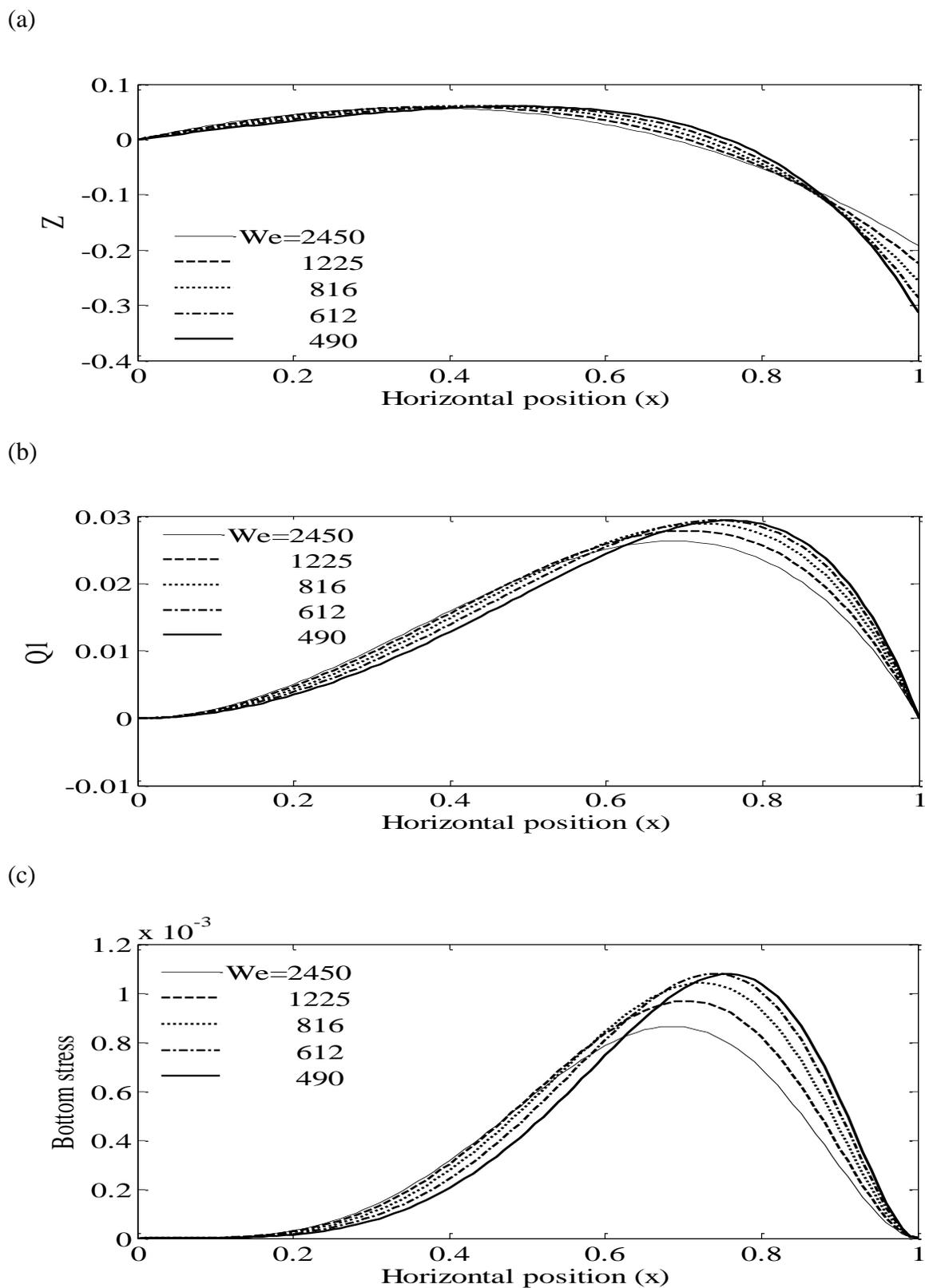
1. Influence of surface tension:

By changing the value of the Weber number (We), the influence of surface tension is examined on the flow field. In this case the aspect ratio, dimensionless wind frequency and wind direction remain fixed.

The figure 3.1(a) represents the variation of the amplitude of the elevation (Z) along the length (horizontal position) of the shallow pond for different values of Weber number (We). The figure is plotted in non-dimensional form, where the horizontal position changes from 0 to 1 in the horizontal direction and the magnitude of the elevation (Z) changes from 0.05 to - 0.30 in the vertical direction of the flow domain. For five values of the (We), a similar behavior is observed for Z. No noticeable change is observed upto a horizontal position of the flow domain, and then there is a sudden decrease in the value of Z along the length of the flow domain. Z shows a downward decrease while moving from left to the right boundary of the flow domain. The zero boundary condition is satisfied at the left lateral boundary of the flow domain.

In figure 3.1(b), the variation of the magnitude of the flow velocity (Q1) is observed with the horizontal position (x) for different values of We. For different values of the We, the value of Q1 increases from the left boundary, attains the peak value at a

distance from the left boundary, and then experiences a sudden decrease to zero at the right boundary of the flow domain to satisfy the lateral boundary condition. The figure is plotted in non-dimensional form, where the horizontal position changes from 0 to 1 in the horizontal direction and the magnitude of the flow velocity (Q1) changes from 0 to 0.029 in the vertical direction of the flow domain. The zero boundary conditions are satisfied at the both lateral boundaries of the flow domain. There is a similarity observed in the behavior of Q1 for high and low values of the We. Although the magnitude of Q1 is not same for different We, but they show a similar pattern for Q1.

(a)

(b)

(c)

Fig3. 1: Influence of surface tension on non-dimensional (a) elevation (Z), (b) flow velocity (Q1) and (c) bottom stress with the horizontal position

Figure 3.1(c) shows the behavior of the bottom stress for different values of We, along the horizontal position (x) of the shallow pond. For different values of the We, the value of the bottom stress increases from the left boundary, attains the peak value at a distance from the left boundary, and then experiences a sudden decrease to zero at the right boundary of the flow domain to satisfy the lateral boundary condition. For five values of the We, a similar behavior is observed for the bottom stress. The figure is plotted in non-dimensional form where the horizontal position changes from 0 to 1 in the horizontal direction and the magnitude of the bottom stress changes from 0 to 1.2×10^{-3} in the vertical direction of the flow domain. The zero boundary conditions are satisfied at the both lateral boundaries of the flow domain. There is a similarity observed in the behavior of the bottom stress for high and low values of the We. Although the magnitude of the bottom stress is different for different We, but they show a similar pattern for the bottom stress. As the bottom stress is the square of Q1, the bottom stress shows the similar pattern as Q1, but the order of magnitude of the bottom stress is different in this case.

2. Influence of inertia:

By changing the value of the Reynolds number (Re_D), the influence of inertia is assessed on the flow field. In this case the aspect ratio, dimensionless wind frequency and wind direction remain fixed.

In figure 3.2(a), elevation (Z) is plotted along the horizontal position of the shallow pond for different values of the Reynolds number (Re_D). The figure is plotted in non-dimensional form, where the horizontal position changes from 0 to 1 in the horizontal direction and the magnitude of the elevation (Z) changes from 0.02 to - 1.5 in the vertical direction of the flow domain. For five values of the Re_D, a similar behavior is observed for Z. No noticeable change is observed upto a horizontal position, and then there is a sudden decrease in the value of Z close to the right boundary of the flow domain. Z shows a downward decrease while moving from left to the right boundary of the flow domain. The zero boundary condition is satisfied at the left lateral boundary of the flow domain.

In figure 3.2(b), the variation of the magnitude of the flow velocity (Q1) is observed with the horizontal position (x) for different values of the Re_D. The figure is plotted in non-dimensional form, where the horizontal position changes from 0 to 1 in the horizontal direction and the magnitude of the flow velocity (Q1) changes from 0 to 0.2 in the vertical direction of the flow domain. For different of value of the Re_D, the value of

(a)

(b)

(c)
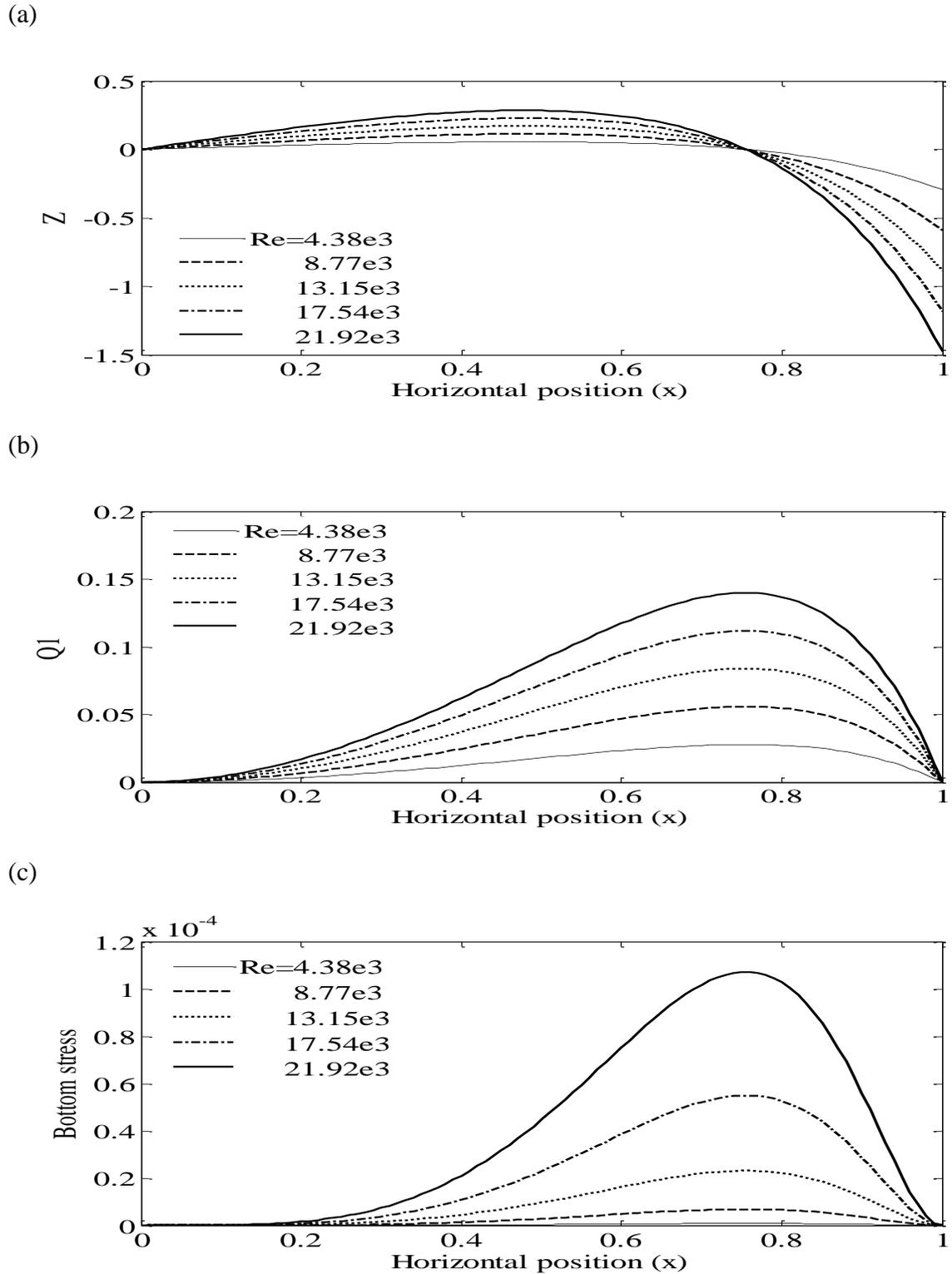
Fig3. 2: Influence of inertia on non-dimensional (a) elevation (Z), (b) flow Velocity (Q1) and (c) bottom stress with the horizontal position

Q1 increases from the left boundary, attains the peak value at a distance from the left boundary, and then experiences a sudden decrease to zero at the right boundary of the flow domain to satisfy the lateral boundary condition. The zero boundary conditions are satisfied at the both lateral boundaries of the flow domain. There is a similarity observed in the behavior of Q1 for high and low value of the Re_D. Although the magnitude of Q1 is not same for different Re_D, but they show a similar pattern for Q1.

Figure 3.2(c) shows the behavior of the bottom stress for different values of the Re_D along the horizontal position of the shallow pond. The figure is plotted in non-dimensional form, where the horizontal position changes from 0 to 1 in the horizontal direction and the magnitude of the bottom stress changes from 0 to 1.2×10^{-4} in the vertical direction of the flow domain. For different values of the Re_D, the values of the bottom stress increases from the left boundary, attains the peak value at a distance from the left boundary, and then experiences a sudden decrease to zero at the right boundary of the flow domain to satisfy the lateral boundary condition. For five values of the Re_D, a similar behavior is observed for the bottom stress. There is a similarity observed in the behavior of the bottom stress for high and low values of the Re_D. Though the magnitude of the bottom stress is different for different Re_D, but they show a similar pattern for the bottom stress. As the bottom stress is the square of Q1, the bottom stress shows the similar pattern as Q1 but the order of magnitude of the bottom stress is different in this case.
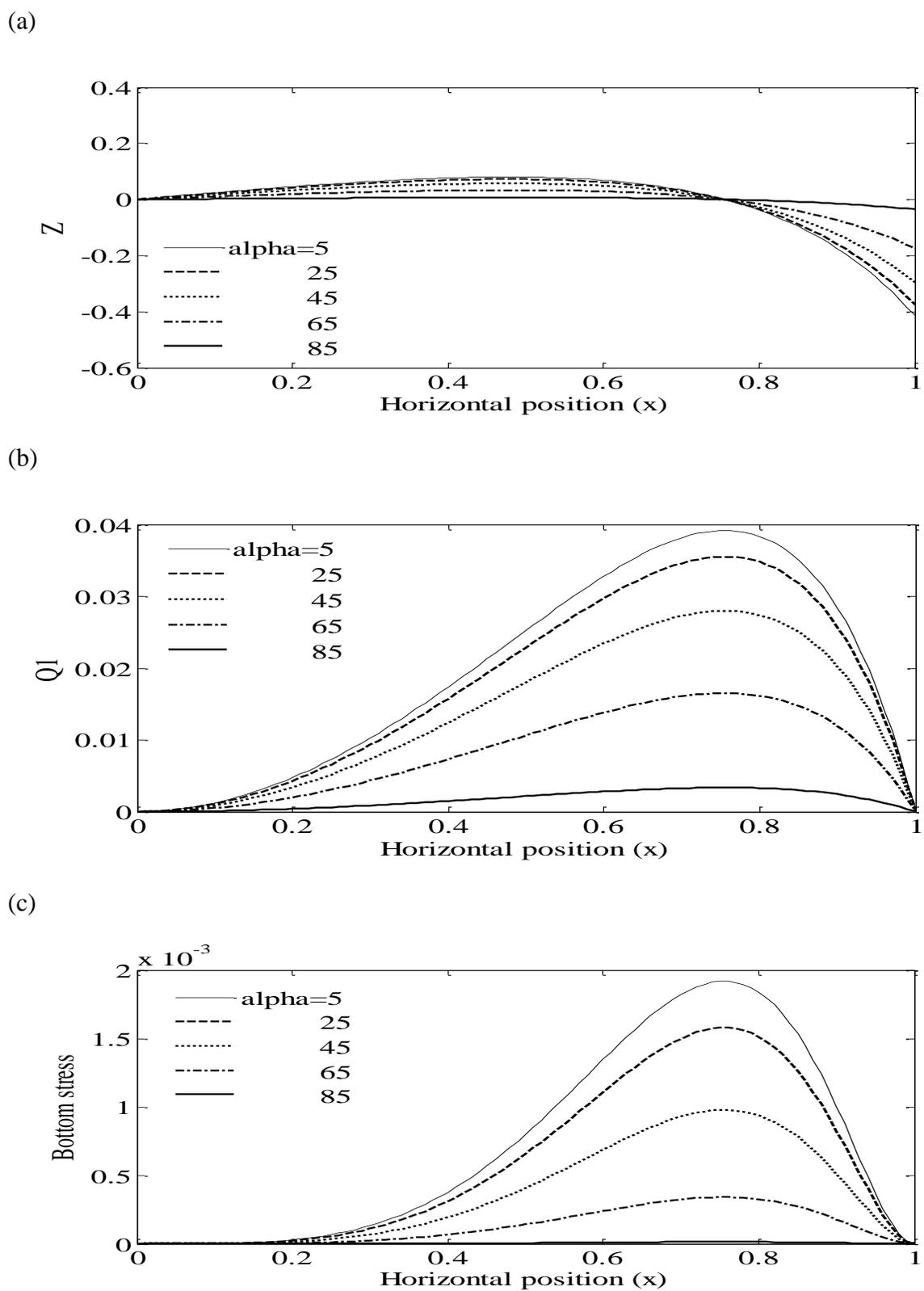
3. Influence of wind direction:

By changing the value of the wind direction alpha (α), the influence of the wind direction is examined on the flow field. By changing the value of α, the wind stress value changes, which is acting over the flow domain to cause resuspension in the shallow pond. In this case the Weber number (We), Reynolds Number (Re_D), aspect ratio and dimensionless wind frequency remain fixed.

Figure 3.3(a) represents the variation of the amplitude of the elevation (Z) along the horizontal position of the shallow pond for different values of α. The figure is plotted in non-dimensional form, where the horizontal position changes from 0 to 1 in the horizontal direction and the magnitude of the elevation (Z) changes from 0.02 to -0.4 in the vertical direction of the flow domain. For different values of α, no noticeable change is observed upto a horizontal position, and then there is a sudden decrease in the value of Z along the length of the flow domain. Z shows a downward decrease while moving from left to the right boundary of the flow domain. The zero boundary condition is satisfied at the left lateral boundary of the flow domain. It is observed as the value of α increases, the value of Z decreases due to lower wind stress influence over the flow domain.

In figure 3.3(b), the variation of Q1 is observed with the position (x) for different values of α. This figure is plotted in non-dimensional form where the horizontal position changes from 0 to 1 in the horizontal direction and the magnitude of the flow velocity (Q1) changes from 0 to 0.039 in the vertical direction of the flow domain. For different values of α, the value of Q1 increases from the left boundary, attains the peak value at a horizontal distance from the left boundary, and then experiences a sudden decrease to

zero at the right boundary of the flow domain to satisfy the lateral boundary condition. The zero boundary conditions are satisfied at the both lateral boundaries of the flow domain. There is a similarity observed in the behavior of Q1 for high and low values of α. Although the magnitude of Q1 is not same for different values of α, but they show a similar pattern for Q1. It is observed from the figure, as the value of α increases, the order of the amplitude of the flow rate (Q1) decreases. This behavior is observed due to low wind stress acting over the flow domain.

Figure 3.3(c) shows the behavior of the bottom stress for different values of α, along the horizontal position of the shallow pond. The figure is plotted in non-dimensional form where the horizontal position changes from 0 to 1 in the horizontal direction and the magnitude of the bottom stress changes from 0 to 2×10^{-3} in the vertical direction of the flow domain. For different values of the $\mathrm{Re_D}$, the value of the bottom stress increases from the left boundary, attains the peak value at a distance from the left boundary, and then experiences a sudden decrease to zero at the right boundary of the flow domain to satisfy the lateral boundary condition. The zero boundary conditions are satisfied at the both lateral boundaries of the flow domain. For different values of α, a similar behavior is observed for the bottom stress. The order of magnitude of the bottom stress decreases as the value of α increases. There is a similarity observed in the behavior of the bottom stress for high and low values of α. Though the magnitude of the bottom stress is different for different $\mathrm{Re_D}$, but a similar pattern is observed for the bottom stress. As the bottom stress is the square of Q1, the bottom stress shows the

(a)

(b)

(c)

Fig3. 3: Influence of wind direction on non-dimensional (a) elevation (Z), (b) flow Velocity (Q1) and (c) bottom stress with the horizontal position

similar pattern as Q1 but the order of magnitude is different in this case. It is demonstrated from the figure, as the value of α increases, the order of magnitude of wind stress decreases.

In this chapter, the influences of the fluid inertia, surface tension and the direction of the wind on the flow field are studied. No significant differences are found for different values of Re_D, We, and α for the flow field at least in appearance, but the magnitude is different for the flow field for high and low values of Re_D, We, and α. As no existing studies have accounted surface tension effect in a shallow tailings pond, no comparison was possible with the results from the present study and the results from the existing studies in a shallow tailings pond. In the present case, the effect of surface tension is considered. The author was mainly interested in observing the effects of fluid inertia, surface tension and wind direction on the flow field and tried to find a behavioral trend of the flow field. The significance and the behavior of the flow field under the influences of fluid inertia, surface tension and wind direction are examined in this chapter. In the next chapter, the problem is formulated without the effect of surface tension and the results from the present analysis are compared with the existing experimental and linear theory results.

CHAPTER 4

COMPARISION WITH EXPERIMENT AND LINEAR THEORY

In this chapter, the problem is formulated without the effect of surface tension to compare and verify the results with linear theory and experimental results. As surface tension is neglected, so it will be assumed that the Weber number value is zero which is included in chapter 2 to formulate the problem. The determined bottom stress from the current study is compared with the bottom stress from linear theory, where the wave period, wave height and wave length are determined using the empirical relations. The influence of the wind comes through the empirical relations for the wave period and wave height in the calculation of the bottom velocity in linear theory. As expected, the magnitude of bottom stress for present study is lower for different water depths compared to linear theory, since viscosity is considered in the present study. It is observed that the bottom stress from the present analysis is of the same order as linear theory and follows the same behavior as linear theory. Moreover, the expression of the flow velocity from linear theory is also formulated in this chapter.

Airy (linear) theory is used in the existing studies, to determine the bottom stress for different water depths at different wind speeds, where the fluid is assumed to be inviscid. In the experimental results, only the critical shear stress for which resuspension will occur is measured with the help of a rotating circular flume in the laboratory (Yanful and Catalan 2002). Bed shear stress applied by the wind induced waves and currents are quite unsteady and rarely can be simulated by mechanical flumes which are done in the laboratory. No published literature was found where the actual wind induced waves and

currents data and corresponding resuspension data have been used to obtain the critical shear stress and erosion rate parameters of the bed tailings. No real time resuspension and wind data were used to determine the erosion rate parameters and the critical shear stress of the bed material. For different wind velocities and water depths, (Yanful and Catalan 2002) were unable to compare experimental results with theoretical (linear theory) results. In their paper they only measured the critical shear stress, which is described as the threshold stress for the resuspension to occur. The measurement gives the value of the minimum bottom stress for which erosion will occur. The onset of the tailings erosion due to wind-induced waves is predicted by comparing the theoretical shear stress (using the bottom velocity expression from linear theory and the empirical relations for wave period, wave height and wave length) with the measured critical shear stress of the tailings. The tailings bed would erode if the theoretical bed shear stress exceeds the measured critical shear stress. Although the bottom stress determination is possible using this present model, but this model cannot determine the critical stress for the onset of resuspension or erosion.

In the next section, the problem is formulated without the effect of surface tension and the results from this present analysis are compared with the results from linear theory and experiment.

4.1 PROBLEM FORMULATION WITHOUT SURFACE TENSION EFFECT

In this section, the governing equations are introduced without the presence of surface tension on the flow field, including the suitable scaling of the constitutive equations as well as the boundary conditions for shallow water flow. The solution procedure is also described in this chapter in some detail.

4.1.1 Problem formulation and boundary conditions for shallow water flow

The conservation of mass and momentum equations (2.1.1 to 2.1.3) remain the same without the effect of surface tension as in chapter 2. The only changes found in the dynamic boundary condition at the free surface due to the absence of surface tension. As the surface tension is neglected in this section, the traction at the free surface in tangential direction (2.1.16) is expressed in dimensional form as (the derivations are similar to chapter 2, upto equation (2.1.16)),

$$T_{XZ} + \frac{H_X}{1 - H_X{}^2}\left(T_{ZZ} - T_{XX}\right) = 0. \tag{4.1.1.1}$$

Similarly, the traction at the free surface in the normal direction (derivations similar from 2.1.16 to 2.1.22) is expressed as

$$P + H_X T_{XZ} - T_{ZZ} = 0. \tag{4.1.1.2}$$

The kinematic boundary condition is also expressed the same way it is expressed in chapter 2 (2.1.23) as,

$$W_H = \frac{dH}{dT} = H_T + UH_X.$$
(4.1.1.3)

4.1.2 Boundary-layer equations for shallow water flow

The scaling method is applied to the dynamic boundary condition (equation 4.1.1.1) in the tangential direction. The boundary condition is expressed in non-dimensional (where the terms of $O\left(\varepsilon^2\right)$ are neglected, similar derivations are followed from 2.2.6 to 2.2.7) form as

$$\tau_{xz} = 0.$$
(4.1.2.1)

Now, the non-dimensional dynamic boundary condition in the normal direction is found, when the scaling is applied to equation (4.1.1.2) as

$$p\left(\frac{\mu U_0}{\varepsilon^2 L}\right) - \frac{\mu U_0}{L}\tau_{zz} = 0.$$
(4.1.2.2)

The expression for the pressure at the free surface is found as

$$p(x, z = h, t) = 0.$$
(4.1.2.3)

This is the dynamic boundary condition in the normal direction at the free surface. The expression for the pressure is found by integrating equation (2.2.5) with respect to z as

$$p = -Gz + c(x, t),$$
(4.1.2.4)

The expression of the hydrostatic pressure becomes

$$p = G(h - z).$$ (4.1.2.5)

Differentiating the pressure with respect to x, equation (4.1.2.5) gives

$$\frac{\partial p}{\partial x} = G \frac{\partial h}{\partial x}.$$ (4.1.2.6)

The expression for first, second derivative of h with respect to x and first derivative of h with respect to t are found as

$$\frac{\partial h}{\partial x} = \frac{\partial \zeta}{\partial x}, \qquad \frac{\partial h}{\partial t} = \frac{\partial \zeta}{\partial t}.$$ (4.1.2.7)

Substituting the expressions of $\frac{\partial h}{\partial x}$ into equation (4.1.2.6), gives the value of the pressure derivative as

$$\frac{\partial p}{\partial x} = p_x = G\zeta_x.$$ (4.1.2.8)

The scaling method is then applied to the kinematic boundary condition (equation 2.2.24) and is expressed in non-dimensional form as

$$w_h = rh_t + uh_x.$$ (4.1.2.9)

Similarly, the kinematic boundary condition at (z = 0) is expressed in non-dimensional form as

$$w_0 = 0.$$ (4.1.2.10)

In this section, as the depth of shallow water flow is very small, using the suitable scaling the governing equations are converted to boundary-layer equations for shallow water flow. In the next section, the effects of the wind and the bottom of the shallow pond are incorporated in the boundary-layer equations for shallow water flow.

4.1.3 Incorporation of the wind conditions and the bottom shear stress

In this section similar to the way of chapter 2, the influences of the wind action and the bottom of the shallow pond come through the wind and bottom stress terms (2.3.1 and 2.3.3) in the boundary-layer equations for shallow water flow. The boundary-layer equations (2.3.14 and 2.3.22) are found by doing the similar derivations from equations (2.3.1 to 2.3.15) are as follow:

$$r\frac{\partial \zeta}{\partial t} + \frac{\partial q}{\partial x} = 0. \tag{4.1.3.1}$$

$$\varepsilon \operatorname{Re_D}\left(rhu_t + uhu_x\right) = -\frac{\partial p}{\partial x}h + \tau_{zx}\big|_{z=h} - \tau_{zx}\big|_{z=0}. \tag{4.1.3.2}$$

Substituting the expressions of the pressure gradient, wind and bottom stress from equations (4.1.2.8) and (2.3.2 and 2.3.4) into equation (4.1.3.2) yields

$$\varepsilon \operatorname{Re_D}\left(rhu_t + uhu_x\right) = -Gh\frac{\partial \zeta}{\partial x} + C_d \operatorname{Re_D}\left(\cos\alpha\right)\cos t - C_b \operatorname{Re_D}\frac{q^2}{h^2}. \tag{4.1.3.3}$$

Now, using the manipulation and simplifications similarly from equations (2.3.17 to 2.3.22), the resultant simplified equation is found as

$$r\frac{\partial q}{\partial t}+\frac{\partial}{\partial x}\left(\frac{q^2}{h}\right)=\frac{1}{\varepsilon\,\mathrm{Re_D}}\left(-\mathrm{Gh}\frac{\partial\zeta}{\partial x}+\mathrm{C_d}\,\mathrm{Re_D}\left(\cos\alpha\right)\cos t-\mathrm{C_b}\,\mathrm{Re_D}\frac{q^2}{h^2}\right). \qquad (4.1.3.4)$$

The boundary conditions at the two lateral boundaries of the shallow pond are given by

$$q\left(x=0,t\right)=q\left(x=1,t\right)=0, \qquad (4.1.3.5)$$

where the boundary conditions describe no-penetration boundary condition at the two lateral boundaries of the shallow pond. In this section, the influences of the wind and the bottom are incorporated in the governing equations through the wind and bottom stress terms. In the next section, the equations (4.1.3.1 and 4.1.3.2) are solved using a small perturbation approach subjected to the boundary conditions (4.1.3.5).

4.1.4. Solution Procedure

In this section, the equations (4.1.3.1 and 4.1.3.2) are solved using a small perturbation approach subjected to the boundary conditions (4.1.3.5). The solution procedure is solved for first order solution only. The boundary conditions and the governing equations are converted to first order to solve the problem. A second order ODE is solved to find the expression of the elevation by solving the governing equations. With the help of the expression of the elevation, the expression of the flow velocity is found using the continuity equation. The expressions of the flow field (elevation, flow velocity and bottom shear stress) are found as the solution of the governing equations (4.1.3.1 and 4.1.3.2).

Now, using the perturbation method similar to chapter 2 and doing the simplifications from equations (2.4.1) to (2.4.5), the equations for first order solution yields

$$r\frac{\partial \zeta_1}{\partial t} = -\frac{\partial q_1}{\partial x}. \tag{4.1.4.1}$$

$$r\frac{\partial q_1}{\partial t} = \frac{1}{\varepsilon \, Re_D}\left(-Gh\frac{\partial \zeta_1}{\partial x} + \frac{C_d \, Re_D (\cos\alpha)\cos t}{\varepsilon}\right). \tag{4.1.4.2}$$

Applying the boundary conditions (4.1.3.5) and neglecting the terms of $O(\varepsilon)$, yields the boundary conditions for the first order solution at the two lateral boundaries of the shallow pond as

$$q_1(x=0,t) = q_1(x=1,t) = 0. \tag{4.1.4.3}$$

Now, equation (4.1.4.2) is differentiated with respect to x, leads to

$$r\frac{\partial}{\partial x}\left(\frac{\partial q_1}{\partial t}\right) = \frac{1}{\varepsilon \, Re_D}\left(-G\frac{\partial^2 \zeta_1}{\partial x^2}\right). \tag{4.1.4.4}$$

Inserting the expression of $\dfrac{\partial q_1}{\partial x}$ from equation (4.1.4.1) into equation (4.1.4.4), results in

$$r\frac{\partial}{\partial t}\left(-r\frac{\partial \zeta_1}{\partial t}\right) = \frac{1}{\varepsilon \, Re_D}\left(-G\frac{\partial^2 \zeta_1}{\partial x^2}\right). \tag{4.1.4.5}$$

Simplifying equation (4.1.4.5) reduces to

$$\frac{\partial^2 \zeta_1}{\partial x^2} - \frac{r^2}{G}\left(\varepsilon \, Re_D \, \frac{\partial^2 \zeta_1}{\partial t^2}\right) = 0. \tag{4.1.4.6}$$

The boundary conditions are also changed and expressed in terms of first order elevation.

Using the boundary condition (4.1.4.3), it is found that $\frac{\partial q_1}{\partial t} = 0$. So, substituting this expression into equation (4.1.4.5) results in

$$G\frac{\partial \zeta_1}{\partial x} = \frac{C_d \operatorname{Re_D}(\cos\alpha)\cos t}{\varepsilon}. \tag{4.1.4.7}$$

Dividing equation (4.1.4.7) with the Gravity number (G), equation (4.1.4.7) reduces to

$$\frac{\partial \zeta_1}{\partial x} = \frac{C_d \operatorname{Re_D}(\cos\alpha)\cos t}{\varepsilon G}. \tag{4.1.4.8}$$

Now, the boundary conditions are expressed in terms of first order elevation as

$$\left.\frac{\partial \zeta_1}{\partial x}\right|_{x=0} = \left.\frac{\partial \zeta_1}{\partial x}\right|_{x=1} = \frac{C_d \operatorname{Re_D}(\cos\alpha)\cos t}{\varepsilon G} = \frac{C_d M(\cos\alpha)\cos t}{\varepsilon^2 r^2}, \tag{4.1.4.9}$$

where, $M = \dfrac{\varepsilon r^2 \operatorname{Re_D}}{G}$.

The most general form of ζ_1 as a solution of equation (4.1.4.6) is expressed as

$$\zeta_1 = Z(x)\cos t. \tag{4.1.4.10}$$

Now, taking the second derivative of ζ_1 with respect to x, t gives

$$\frac{\partial^2 \zeta_1}{\partial x^2} = \frac{d^2 Z}{dx^2}\cos t, \qquad \frac{\partial^2 \zeta_1}{\partial t^2} = Z(-\cos t). \tag{4.1.4.11}$$

Inserting the expressions from equation (4.1.4.11) into equation (4.1.4.6) to express equation (4.1.4.6) in terms of Z leads to,

$$\left(\frac{d^2 Z}{dx^2} + \frac{\varepsilon r^2 \, Re_D}{G} Z \right) \cos t = 0. \tag{4.1.4.12}$$

From equation (4.1.4.12), one ODE is found in terms of Z, namely

$$\left(\frac{d^2 Z}{dx^2} + MZ \right) = 0. \tag{4.1.4.13}$$

Solution of equation (4.1.4.13) takes the following form

$$Z = A \cos(\sqrt{M} x) + B \sin(\sqrt{M} x). \tag{4.1.4.14}$$

Now, with the help of equation (4.1.4.14), the first derivative of Z with respect to x is found as

$$\frac{dZ}{dx} = -\sqrt{M} A \sin(\sqrt{M} x) + \sqrt{M} B \cos(\sqrt{M} x). \tag{4.1.4.15}$$

Inserting the values of x = 0, 1 into equation (4.1.4.15), equation (4.1.4.15) reduces to

$$\left. \frac{dZ}{dx} \right|_{x=0} = \sqrt{M} B. \tag{4.1.4.16}$$

$$\left. \frac{dZ}{dx} \right|_{x=1} = -\sqrt{M} A \sin(\sqrt{M}) + \sqrt{M} B \cos(\sqrt{M}). \tag{4.1.4.17}$$

To find the values of the constants (A, B) in equation (4.1.4.14), two boundary conditions are required in terms of Z. Now the boundary conditions expressed in terms of first order elevation (4.1.4.9) are expressed in terms of Z as

$$\left(\frac{dZ}{dx}\right)\Bigg|_{x=0}\cos t = \frac{C_d M(\cos\alpha)\cos t}{\varepsilon^2 r^2}.$$

(4.1.4.18)

$$\left(\frac{dZ}{dx}\right)\Bigg|_{x=1}\cos t = \frac{C_d M(\cos\alpha)\cos t}{\varepsilon^2 r^2}.$$

(4.1.4.19)

Equating the co-efficient of cost of equation (4.1.4.18) results in

$$\sqrt{M}B = \frac{C_d M(\cos\alpha)}{\varepsilon^2 r^2} \Rightarrow B = \frac{C_d \sqrt{M}(\cos\alpha)}{\varepsilon^2 r^2}.$$

(4.1.4.20)

Similarly, equating the co-efficient of cost of equation (4.1.4.19) reduces to

$$-\sqrt{M}A\sin(\sqrt{M}) + \sqrt{M}B\cos(\sqrt{M}) = \frac{C_d M(\cos\alpha)}{\varepsilon^2 r^2}.$$

(4.1.4.21)

Simplifying equation (4.1.4.21) and using the expression of B from equation (4.1.4.20) into equation (4.1.4.21) results the expression of A as

$$A = -\frac{C_d \sqrt{M}(\cos\alpha)}{\varepsilon^2 r^2}\tan\frac{\sqrt{M}}{2}.$$

(4.1.4.22)

Inserting the expressions of A and B into equation (4.1.4.14), gives the expression of Z as,

$$Z = -\frac{C_d \sqrt{M}(\cos\alpha)}{\varepsilon^2 r^2}\left(\tan\frac{\sqrt{M}}{2}\cos(\sqrt{M}x) - \sin(\sqrt{M}x)\right). \qquad (4.1.4.23)$$

After substituting the expression of Z into equation (4.1.4.10), the expression of the first order elevation is found. It is found that the first order elevation depends only on cost contribution.

$$\zeta_1 = -\frac{C_d \sqrt{M}(\cos\alpha)}{\varepsilon^2 r^2}\left(\tan\frac{\sqrt{M}}{2}\cos(\sqrt{M}x) - \sin(\sqrt{M}x)\right)\cos t. \qquad (4.1.4.24)$$

Now, substituting the expression of ζ_1 into equation (2.4.1a), the expression of the elevation becomes

$$\zeta = \varepsilon\zeta_1 = -\frac{C_d \sqrt{M}(\cos\alpha)}{\varepsilon r^2}\left(\tan\frac{\sqrt{M}}{2}\cos(\sqrt{M}x) - \sin(\sqrt{M}x)\right)\cos t. \qquad (4.1.4.25)$$

Now, inserting the expression of the first order depth integrated velocity (q_1) as $q_1 = Q_1 \sin t$ into equation (4.1.4.1) leads to

$$rZ(-\sin t) = -\frac{dQ_1}{dx}(\sin t) \Rightarrow rZ = \frac{dQ_1}{dx}. \qquad (4.1.4.26)$$

Integrating equation (4.1.4.26) with respect to x between 0 to x, the expression for Q_1 is found as,

$$Q_1 = r\int_0^x Z dx = \int_0^x -\frac{C_d \sqrt{M}(\cos\alpha)}{\varepsilon^2 r}\left(\tan\frac{\sqrt{M}}{2}\cos(\sqrt{M}x) - \sin(\sqrt{M}x)\right)dx. \qquad (4.1.4.27)$$

So, the expression for the first order depth integrated velocity becomes,

$$q_1 = Q_1 \sin t = -\frac{C_d (\cos \alpha)}{\varepsilon^2 r} \left(\sec \frac{\sqrt{M}}{2} \cos(\frac{1}{2}\sqrt{M}(1-2x)) - 1 \right) \sin t. \qquad (4.1.4.28)$$

Now, using the expression of q_1 from equation (4.1.4.28) into equation (2.4.1b), results the expression for the depth integrated velocity (flow rate) as

$$q = -\frac{C_d (\cos \alpha)}{\varepsilon r} \left(\sec \frac{\sqrt{M}}{2} \cos(\frac{1}{2}\sqrt{M}(1-2x)) - 1 \right) \sin t. \qquad (4.1.4.29)$$

Using the expressions ζ_1, q_1 found earlier, the calculation of the flow field is done. Flow velocity is found dividing the depth integrated velocity/flow rate (q) with the depth of water (h) of the shallow pond. Substituting the expression of $q_1 = u_1 h = u_1 (1 + \varepsilon \zeta_1)$ into equation (4.1.4.28) reduces to

$$u_1 h = u_1 (1 + \varepsilon \zeta_1) = -\frac{C_d (\cos \alpha)}{\varepsilon^2 r} \left(\sec \frac{\sqrt{M}}{2} \cos(\frac{1}{2}\sqrt{M}(1-2x)) - 1 \right) \sin t. \qquad (4.1.4.30)$$

So, the expression of the flow velocity becomes,

$$u = \varepsilon u_1 = -\frac{C_d (\cos \alpha) \sin t}{\varepsilon r (1 + \varepsilon \zeta_1)} \left(\sec \frac{\sqrt{M}}{2} \cos(\frac{1}{2}\sqrt{M}(1-2x)) - 1 \right). \qquad (4.1.4.31)$$

Now, the expression of the bottom stress is found from equation (2.3.7) as

$$\tau_b = C_b \, Re_D \, u^2.$$

Substituting the expression of u from equation (4.1.4.1.31) leads to

$$\tau_b = C_b \, Re_D \, u^2 = C_b \, Re_D \left(-\frac{C_d (\cos \alpha) \sin t}{\varepsilon r (1 + \varepsilon \zeta_1)} \left(\sec \frac{\sqrt{M}}{2} \cos(\frac{1}{2} \sqrt{M} (1 - 2x)) - 1 \right) \right)^2 .(4.1.4.32)$$

This is the expression of the bottom stress of the shallow pond. In this section, a small perturbation method is used to solve the problem and finally, the expressions for the elevation, flow velocity and bottom stress are found as the solution of the problem. In the next section, the expression of the bottom stress due to wind waves using linear wave theory is formulated.

4.2 Calculation of the bottom shear stress due to wind waves using linear wave theory:

As the main cause of the motion in shallow ponds is wind, some emphasis should be placed on the measurement of the wind velocity and the wind-induced waves. Most authors use the Sverdrup Munk Bretschneider (SMB) equations to calculate the wave heights, and hence the bottom shear stresses (Adu Wusu et al., 2001; Yanful and Catalan 2002). Only a few studies have been conducted in shallow lakes to measure and compare the actual wave heights (Berbner and Sangal, 1964; Sheng and Lick, 1979) with those predicted from the existing equations. In addition, most of these studies have been conducted in lakes, which are much deeper than mine tailings ponds. Previous studies (Pickens and Lick 1992; Whitehouse et al. 1999; Yang et al. 2000) have shown that resuspension is very much dependent on the frictional shear force exerted by the flow per unit area of bed, known as the bed shear stress. To calculate the bed shear stresses generated at the bottom of the water cover by wind-induced waves, wave characteristics

were determined using the wave hindcasting formulae based on the Sverdrup-Munk-Bretschneider (SMB) method for shallow water waves (U.S. Army Coastal Engineering Research Centre 1984). The significant wave height H_1, significant wave period T_1 and significant wavelength L_1 can be calculated by the following empirical equations:

$$H_1 = \left(\frac{U^2_A}{g} \right) 0.283 \tanh \left[0.53 \left(\frac{gh}{U^2_A} \right)^{0.75} \right] \times \tanh \left\{ \frac{.00565 \left(\frac{gF}{U^2_A} \right)^{0.5}}{\tanh \left[0.53 \left(\frac{gh}{U^2_A} \right)^{0.75} \right]} \right\}. \qquad (4.2.1)$$

$$T_1 = \left(\frac{U_A}{g} \right) 7.54 \tanh \left[0.833 \left(\frac{gh}{U^2_A} \right)^{0.375} \right] \times \tanh \left\{ \frac{.0379 \left(\frac{gF}{U^2_A} \right)^{0.25}}{\tanh \left[0.833 \left(\frac{gh}{U^2_A} \right)^{0.375} \right]} \right\}. \qquad (4.2.2)$$

$$L_1 = \frac{gT^2_1}{2\pi} \tanh \left(\frac{2\pi h}{L_1} \right). \qquad (4.2.3)$$

In equations (4.2.1-4.2.3), U_A is the wind stress factor ($=0.71 U^{1.23}$, where U is the wind speed in (m/s) blowing at a reference height over the flow domain, h is the depth of water and F is the fetch of the shallow pond. In the next section, the derivation of the horizontal bottom velocity from the linear wave theory is done.

4.2.1 Calculation of the horizontal bottom velocity from the linear wave theory:

In this section, the horizontal bottom velocity from the linear wave theory is derived. The linear wave theory (Airy 1845) is the 2-D; simplest and the most useful

wave theory in the literature. The theory assumes the fluid to be inviscid and the surface tension is also neglected in this theory. The figure (4.2.1) shows the three types of boundary conditions which are used in the linear wave theory to derive the expression of the horizontal bottom velocity. In this figure, H_1 and L_1 represent the significant wave height and significant wave length and η shows the elevation from the axis, where the elevation depends upon position and time. Some assumptions are considered in the linear wave theory for the calculations of the horizontal bottom velocity are as follow:

1. Fluid is homogenous and incompressible.

2. Coriolis effect is neglected.

3. Fluid is inviscid (no viscosity).

4. Surface Tension forces are negligible.

5. Flow is irrotational.

6. Bottom is horizontal, stationary and impermeable.

7. Waves are two dimensional (long crested).

8. Waves do not interact with other water motion.

9. Surface pressure is constant.

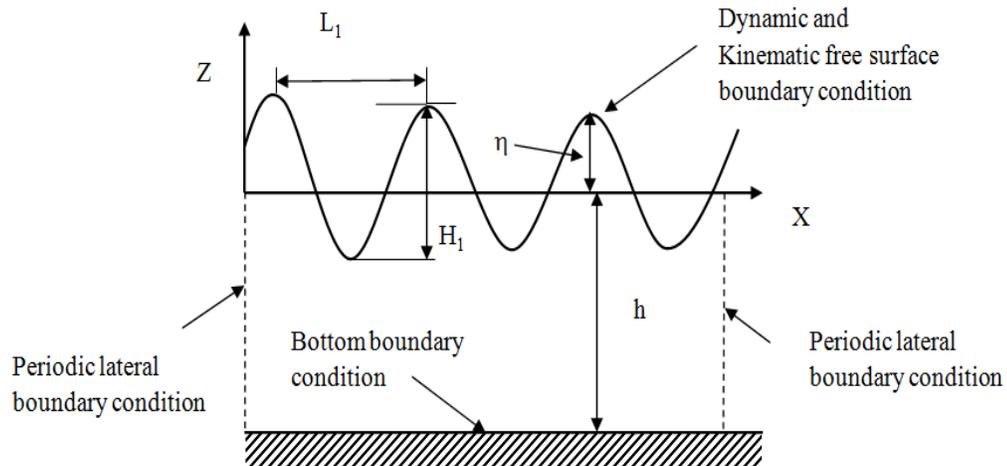10. Wave amplitude is small compared to the wavelength and water depth.

Fig 4.2.1 Three types of boundary conditions and the significant wave height and significant wavelength used in linear wave theory for the calculation of the bottom velocity.

In this section, the expression for bottom velocity in a shallow tailings pond is formulated using the linear theory. (Water wave mechanics for engineers and scientists by Robert G. Dean and Robert A.Dalrymple, 1984). In linear wave theory for an incompressible fluid, two dimensional motions in the X, Z plane are given by,

$$\frac{\partial U}{\partial X} + \frac{\partial W}{\partial Z} = 0. \tag{4.2.1.1}$$

As it is assumed that the flow is irrotational in linear theory, then a velocity potential exists which by definition gives

$$U = -\frac{\partial \phi}{\partial X}, \quad \text{and} \quad W = -\frac{\partial \phi}{\partial Z}. \tag{4.2.1.2}$$

Using the relations (4.2.1.2) into equation (4.2.1.1), equation (4.2.1.1) reduces to

$$\frac{\partial^2 \phi}{\partial X^2} + \frac{\partial^2 \phi}{\partial Z^2} = 0. \tag{4.2.1.3}$$

For an incompressible fluid of the irrotational motion, the governing equations in the X-Z plane are the Euler equations, expressed in dimensional form as

$$\frac{\partial U}{\partial T} + U \frac{\partial U}{\partial X} + W \frac{\partial U}{\partial Z} = -\frac{1}{\rho} \frac{\partial P}{\partial X}. \tag{4.2.1.4}$$

$$\frac{\partial W}{\partial T} + U \frac{\partial W}{\partial X} + W \frac{\partial W}{\partial Z} = -\frac{1}{\rho} \frac{\partial P}{\partial Z} - g. \tag{4.2.1.5}$$

Due to the fact that the pressure on the free surface ($Z = \eta$) is zero. So, the free surface boundary condition is obtained as

$$\eta = \frac{1}{g}\left[\frac{\partial \phi}{\partial T}\right]_{Z=\eta}.$$

As waves are small, it is assumed that the satisfying boundary condition at the free surface $(Z = \eta)$ will be equal to the boundary condition at $(Z = 0)$

$$\therefore \eta = \frac{1}{g}\frac{\partial \phi}{\partial T} \qquad \text{on } Z = 0 \tag{4.2.1.6}$$

In linear wave theory, it is assumed that the velocity at the bottom boundary is equal to zero due to non-penetration condition. The bottom boundary condition is expressed as

$$W = -\frac{\partial \phi}{\partial Z} \qquad \text{on } Z = -h \tag{4.2.1.7}$$

The waves are assumed to be periodic in space and time. So, the lateral boundary condition is expressed as a periodicity condition as,

$$\phi(X,T) = \phi(X+L_1,T),$$
$$\phi(X,T) = \phi(X,T+T_1),$$

(4.2.1.8)

where L_1 is the significant wavelength and T_1 is the significant wave period. A powerful method for the solution of the partial differential equations is to use the separation of variables in which a solution is assumed in product form, each term of the product being only a function of one of the independent variables. For the solution of equation (4.2.1.3), the ϕ is taken as the form

$$\phi(X,Z,T) = X(X)Z(Z)T(T),$$

(4.2.1.9)

where X is a function depends only on X, Z depends only on Z and T varies only with time. As it is known, that ϕ must be periodic in time by the lateral boundary condition; so (T) can be specified as $T(T) = \sin \sigma_1 T$, where σ_1 is the angular frequency of the wave. So, equation (4.2.1.9) leads to

$$\phi(X,Z,T) = X(X)Z(Z)\sin \sigma_1 T.$$

(4.2.1.10)

Doing the manipulations and simplifications, the final expression of ϕ is expressed as

$$\phi = -\frac{H_1 g}{2\sigma_1} \frac{\cosh k(h+Z)}{\cosh kh} \sin(kX - \sigma_1 T).$$

(4.2.1.11)

Now, to calculate the flow velocity the relation (4.2.1.2) is used as

$$U = -\frac{\partial \phi}{\partial X} = \frac{H_1 k}{2} \frac{g \cosh k(h+Z)}{\sigma_1 \cosh kh} \sin(kX - \sigma_1 T). \qquad (4.2.1.12)$$

Using the expression of the wave number $\left(k = \frac{2\pi}{L_1} \right)$, equation (4.2.1.12) reduces to

$$U = \frac{\pi H_1}{L_1} \frac{g \cosh k(h+Z)}{\sigma_1 \cosh kh} \cos(kX - \sigma_1 T). \qquad (4.2.1.13)$$

The time period is given by $T_1 = \frac{L_1}{C} = L_1 \times \frac{\sigma_1}{g} \times \frac{1}{\tanh kh}$, so the expression of the bottom

velocity with time period is expressed as

$$U = \frac{\pi H_1}{T_1} \frac{\cosh k(h+Z)}{\sinh kh} \cos(kX - \sigma_1 T). \qquad (4.2.1.14)$$

For shallow water flow, it is assumed that $\cosh k(h+Z)=1$ and if the wave move such that

at all time (T), position relative to the wave remains fixed. Therefore, $kX - \sigma_1 T$

=constant. The final expression for the bottom velocity in shallow water flow is given by

$$U_{bm} = \frac{\pi H_1}{T_1} \frac{1}{\sinh kh} = \frac{\pi H}{T} \frac{1}{\sinh\left(\frac{2\pi}{L_1}h\right)}. \qquad (4.2.1.15)$$

where the significant wave height (H_1), significant wavelength (L_1) and significant wave

period (T_1) can be determined using the empirical relations (4.2.1-4.2.3). Therefore, the

bottom velocity just above the tailings pond U_{bm} becomes, $U_{bm} = \frac{\pi H}{T_1} \left[\frac{1}{\sinh\left(\frac{2\pi}{L_1}h\right)} \right]$

The oscillatory bottom shear stress due to waves from the published work (Jonsson 1966) τ_w can be calculated from the bottom velocity as follows:

$$\tau_w = \frac{1}{2} f_w \rho U^2_{bm},$$
(4.2.1.16)

where f_w is the wave friction factor, ρ is the fluid density, and U_{bm} is bottom fluid velocity near the tailings bed. The wave friction factor f_w is a function of the amplitude Reynolds number $\left(R_w\right)$ and the relative roughness of the boundary. For laminar flow, f_w is given by, $f_w = \dfrac{2}{\sqrt{R_w}}$. The amplitude Reynolds number $\left(R_w\right)$ is defined by,

$R_w = \dfrac{U_{bm} a_m}{\upsilon}$; where a_m is the maximum displacement of the individual fluid particles from their mean position and $\upsilon$ the kinematic viscosity of the fluid. Here, a_m is given by, $a_m = \dfrac{H_1}{2 \sinh\left(\dfrac{2\pi h}{L_1}\right)}$.

4.3 Comparison with experiment and linear theory:

In this section, the results from the present analysis are compared with experimental and linear theory results. Though the wind condition in present model and in linear wave theory is not same, the results from the present analysis show a similar behavior with linear theory and experimental results. The wind is taken as periodic and at an angle with the x-axis in present model while it is assumed that wind is steady and parallel to the flow domain in linear theory. The elevation, flow velocity and bottom stress are plotted along the length of the shallow pond without the effect of surface tension. The effect of surface tension is neglected in this chapter to compare the results with the existing available results, where the effect of surface tension is not examined. The present analysis is different from linear theory as viscous effect is ignored in linear theory, whereas it is considered in the present analysis. The variation of the elevation, flow velocity and bottom stress are plotted with the horizontal position of the flow domain. The study can be extended for any other shallow or thin-film application, where viscosity is different from water.

In figure (4.3.1), the elevation is plotted with the horizontal position of the shallow pond in dimensional from. The water depth of 0.5 (m) and wind velocity of 10 (m/s) blowing at a reference height of 10 (m) over the length of the shallow pond is considered in this analysis. In the horizontal direction, the position differs from 0 (m) to 1500 (m) and the elevation changes from -0.0564 (m) to 0.0564 (m) in the vertical direction of the flow domain. Though the wind acting over the flow domain is not periodic with respect to position, but the figure (4.3.1) shows a periodic behavior for elevation along the position of the flow domain. At the left boundary of the flow domain,

the elevation starts from a negative value and it reaches a maximum value of around 0.0564 (m) and minimum value of -0.0564 (m). Since the length of the pond is small, the highest and lowest value of the elevation remains constant throughout the flow domain. No significance difference is found in the value of the elevation along the length of the flow domain.
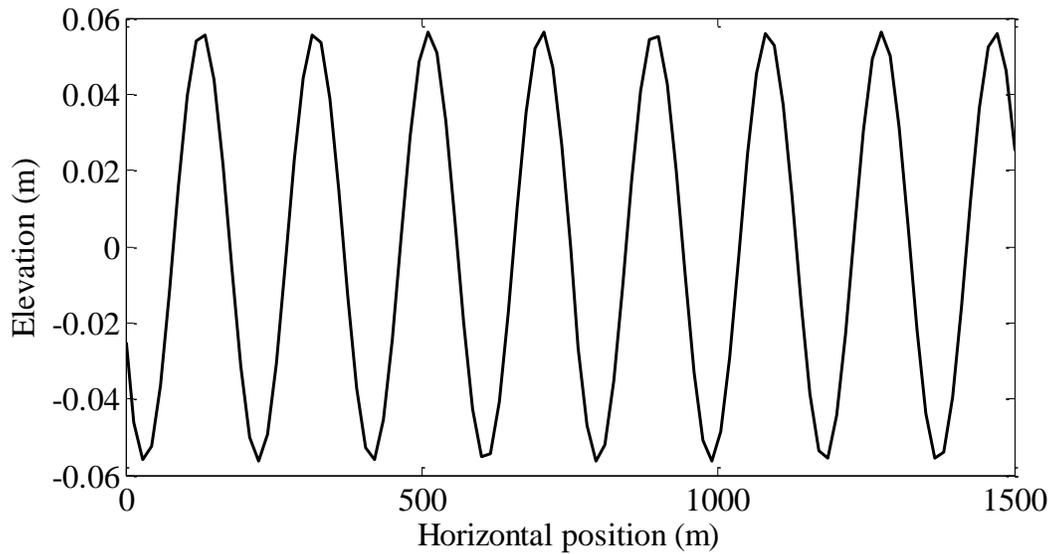
Fig4.3. 1 Variation of the elevation with the horizontal position of the shallow pond

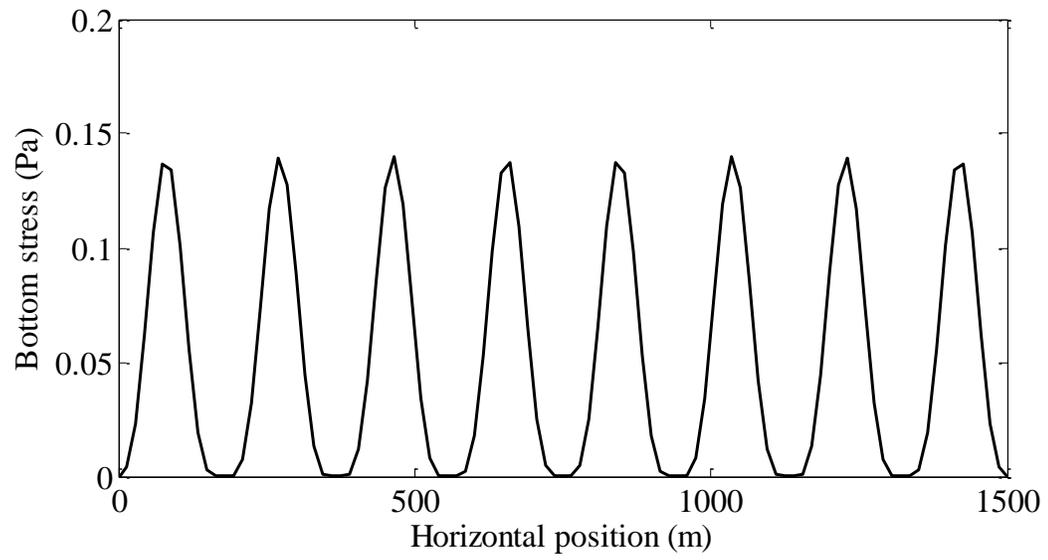Figure (4.3.2) demonstrates the variation of flow velocity in (m/s) with the horizontal position (m) of the shallow pond. The water depth of 0.5 (m) and a wind velocity of 10 (m/s) blowing at a reference height of 10 (m) over the length of the shallow pond is considered in this analysis. The position changes from 0 (m) to 1500 (m) in the horizontal direction, while the flow velocity changes from 0.4728 (m/s) to -0.0263 (m/s) in the vertical direction of the flow domain. The zero boundary conditions due to no-penetration condition are satisfied at the two lateral boundaries of the flow domain. At the left boundary of the flow domain, the flow velocity starts from zero value to satisfy the lateral boundary condition and it reaches a maximum value of around 0.4728 (m/s) and minimum value of -0.0263 (m/s). The highest and lowest value of the flow velocity remains constant throughout the flow domain, due to the small length of the pond for a variation in the value of the flow velocity. In this study, the determined average value of the flow velocity along the length of the pond, found to be around 0.24 (m/s). The calculated flow velocity from linear theory (4.2.1.30) is found to be around 0.24 (m/s) for a water depth of 0.5 (m) and wind velocity of 10 (m/s) acting over the shallow pond. It is observed, that the results from the present analysis demonstrate better agreement with linear theory results for calculating the flow velocity. Although the wind acting over the flow domain is not periodic with respect to position, but this figure shows a periodic behavior for flow velocity along the position of the flow domain. As the flow velocity does not change in the vertical direction/with respect to the height of the shallow pond, therefore, the calculated flow velocity is taken as the bottom velocity to determine the bottom stress, where the bottom stress depends upon the bottom velocity.
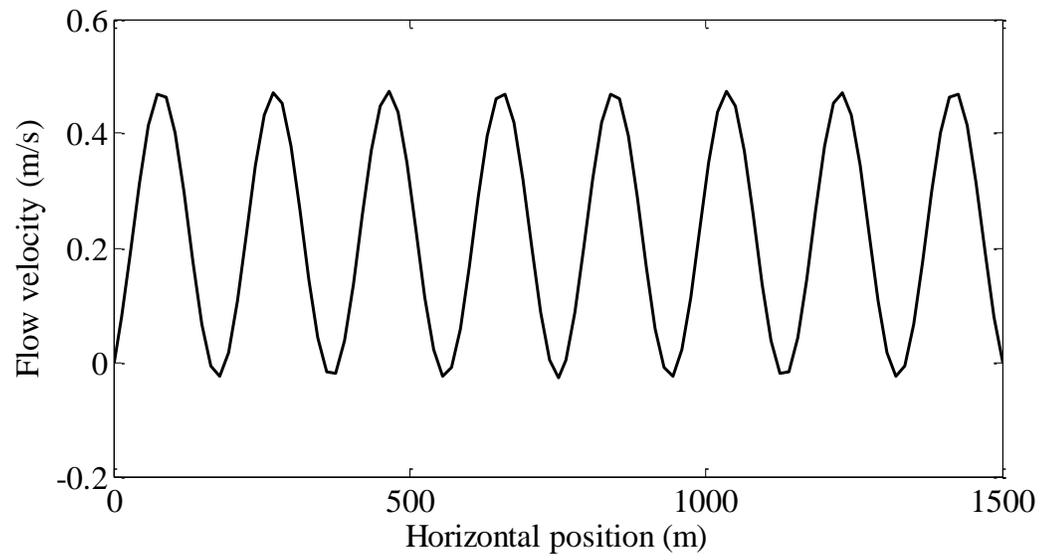
Fig4.3. 2 Variation of the flow velocity with the horizontal position of the shallow

pond

The variation of bottom stress (Pa) along the horizontal position (m) of the shallow pond is illustrated in figure (4.3.3). The figure is plotted for a water depth of 0.5 (m), and a wind velocity of 10 (m/s) blowing at a height of 10 (m) over the length of the shallow pond. The horizontal position changes from 0 (m) to 1500 (m) in the horizontal direction, while the bottom stress changes from 0.1397 (Pa) to 0 (Pa) in the vertical direction of the flow domain. Though the wind acting over the flow domain is not periodic with respect to position, but this figure shows a periodic behavior for bottom stress along the position of the flow domain. The zero boundary conditions due to no-penetration condition are satisfied at the two lateral boundaries of the flow domain. At the left boundary of the flow domain, the bottom stress starts from zero value to satisfy the lateral boundary condition and it reaches a maximum value of around 0.1397 (Pa) and minimum value of 0 (Pa). Due to small length of the pond, the highest and lowest value of the bottom stress remains almost of the same order throughout the flow domain.

Fig4.3. 3 Variation of the bottom stress with the horizontal position of the shallow
pond

Figure (4.3.4) demonstrates the variation of bottom stress for different water depths of h=0.5m,1m,1.5m and 2 m in a shallow pond for a wind velocity of $U_0 = 10$ m/s acting over the shallow pond. The figure shows the variation of bottom stress (Pa) for different water depths (m), from three different approaches to compare the bottom stress values with one another. The bottom stress from the three approaches that are plotted in this figure are; linear (Airy 1845) wave theory, critical stress from experimental value (Yanful and Catalan 2002) and the present study. As expededed, the figure shows that as the depth of the water increases, the bottom stress decreases and for higher water depth there is less chance of resuspension or erosion of tailings. Although deep water covers induce less bottom stress in a shallow pond, but as it is known that deep water covers are not favorable due to geotechnical stability, construction and maintanence cost. That is why shallow water covers are used in place of deep water covers in shallow mine tailings pond. When the critical stress value is small, there is more chance of resuspension as resuspension will occur when the calculated bottom stress (linear wave theory and present study) exceeds the critical shear stress. Thus, the onset of resuspension depends on the critical value of the bottom stress. It is observed that the bottom stress for the present analysis is lower compared to linear wave theory, since viscosity is added in the present analysis. The order of bottom stress from the present analysis is of the same order as linear wave theory and the figure (4.3.4) follows the same behavior as linear wave theory. At a depth of h=0.5 (m) and wind velocity of 10 (m/s), it is observed that the bottom stress is 0.61 (Pa) from linear wave theory, whereas 0.175 (Pa) from the present study. The critical stress is found to be around 0.17 (Pa) from the experimental values

(Yanful and Catalan 2002), where the experiment is done with the help of a rotating circular flume in a laboratory.
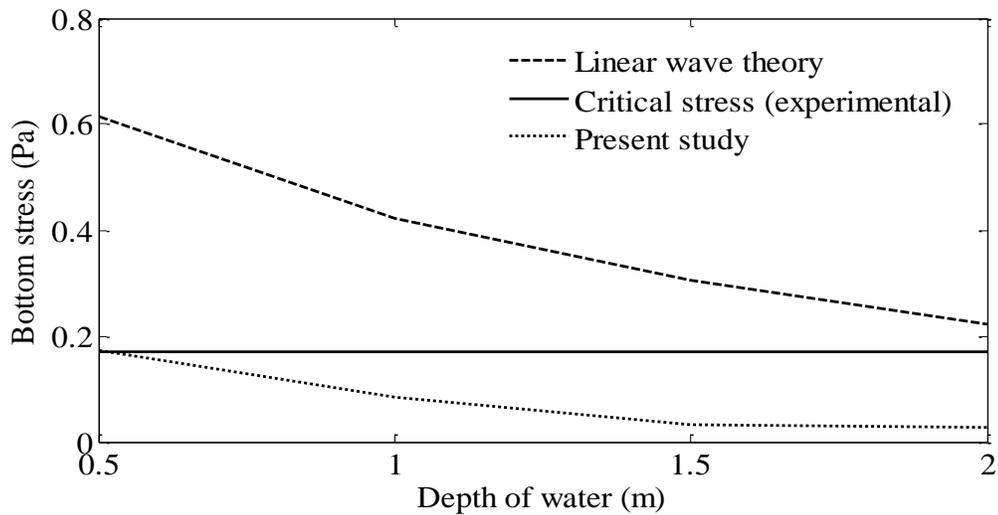
Fig4.3. 4: Variation of the bottom stress with depth of water in the shallow pond for linear theory, experimental result and present study

In this chapter, the problem is formulated similar to chapter 2 but the surface tension effect is neglected. The expression of bottom velocity from linear wave theory is summarized in this chapter. In this case, the wave height and the wave length need not to be determined from the empirical relations, which reduce the computations required for the calculation of the bottom stress. The results from the present analysis are compared with linear theory and experimental results and it was observed that this present analysis can be used as an alternative approach for predicting the bottom stress in a shallow pond.

CHAPTER 5

CONCLUSION

5.1 Concluding remarks and Summary

The prediction of bottom shear stresses in a shallow mine tailings pond is examined in this study. Although the study is considered in a shallow mine tailings pond, the study can be extended for the prediction of bottom stress in any other shallow or thin-film application. Two cases, with and without the effect of surface tension on the flow field are considered in this study. The results without the effect of surface tension from this present study are compared with linear theory and experimental results. The problem is of direct relevance to the wind-wave induced resuspension of mine tailings in disposal ponds, where the prediction of bottom stress is determined with the help of linear theory and the empirical relations for the significant wave period, significant wave height and significant wave length. In the present study, the boundary-layer equations for shallow water flow are derived following the suitable scaling of mass and momentum conservation equations, and are solved by a small perturbation method. Finally, the elevation, flow velocity and bottom stress are determined along the horizontal position of the shallow pond. Moreover, the average bottom stress values along the position are determined for different water depths at a specific wind speed, and the bottom stress values are compared with the bottom stress values from linear theory and experiment. The prediction of the bottom stress values from this study shows a better agreement with the existing (linear theory and experiment) bottom stress values to verify the present

study. A number of assumptions are made in the current study, which must be relaxed for more realistic predictions to be reached.

In chapter - 1 (Introduction), the study is focused on the thin-film or shallow flow applications found in the literature. The characteristics and applications of shallow water flow are described in this chapter. Some previous studies on thin-film flow where surface tension was considered are described in this chapter. As we are mainly focusing our attention in shallow flow, so previous studies of the resuspended flooded mine tailings ponds in the literature are also described in this chapter. This chapter has demonstrated the significance of the present study as well as relevance of the present study to reality. Moreover, it describes how this study can be an alternative choice for predicting the bottom shear stress in a shallow mine tailings pond considering viscous and surface tension effects. This chapter describes the significance of the bottom stress in shallow water flow compared to deep water flow. The benefits and significances of shallow water covers compared to deep water covers are also illustrated in this chapter.

Chapter - 2 (General Problem formulation) describes the fundamental equations, (conservation of mass and momentum) considering the viscous and surface tension effects for shallow water flow. The boundary-layer equations for shallow water flow are obtained using the suitable scaling method. The influence of surface tension comes through the dynamic boundary condition at the free surface of the flow field. The governing equations are simplified by omitting the coriolis and the eddy viscosity terms and using the empirical relations for wind and bottom stresses. Three types of boundary conditions are used to solve the problem:

1. Free surface boundary condition:

    (a) Dynamic boundary condition which demonstrates the force balance at the free surface.

    (b) Kinematic Boundary condition which relates the motion of the free interface to the fluid velocities at the free surface.

2. Bottom Boundary Condition: This boundary condition describes the vertical velocity at the bottom is zero due to no-penetration condition.

3. Lateral boundary Conditions: These conditions describe the flow velocities are zero due to no-penetration condition at the two lateral confined boundaries. This boundary condition also demonstrates that the elevation is zero at the left boundary of the flow domain, when considering the effect of surface tension in the problem formulation.

    A small perturbation method is used to solve the governing equations, where it is assumed that the elevation is an order of magnitude smaller than the depth of water and the problem is solved for the first order solution only. Therefore, the boundary conditions are also changed for the first order solution. The influences of the wind and the bottom of the shallow pond are inserted through the empirical relations for wind and bottom stresses in the problem formulation. Finally, the expressions for the elevation, flow velocity and bottom stress are found as the solution to the problem.

    Chapter - 3 (Influence of inertia and surface tension) demonstrates the influences of fluid inertia, surface tension and wind direction on the flow field in the present study. In the current study, the Reynolds number (Re_D), the Weber number (We) and the wind

direction (α) are varied to study the flow field (elevation, flow velocity and bottom stress). As no existing studies have accounted surface tension effect in shallow tailings pond, no comparison was possible with the results from the present study and the results from the existing studies. In the present case, the effect of surface tension is considered. The author was mainly interested in observing the effects of fluid inertia, surface tension and wind direction on the flow field and tried to find a behavioral trend of the flow field. The significance and the behavior of the flow field under the influences of fluid inertia, surface tension and wind direction are examined in this chapter.

In chapter - 4 (Comparison with experiment and linear theory), the results without the effect of surface tension from the present study are compared with the existing results, where the flow velocity is determined using the linear theory. Both analyses show the same qualitative and quantitative results for the bottom stress, while using different water depths of the shallow pond. As expected, the bottom stress values from the present study are lower compared to the bottom stress values from linear theory. This behavior is observed as viscosity is considered in the present study. With the present study, it is observed that the predicted bottom stress value is of the same order bottom stress value from linear theory and follows the same behavior as linear theory. Moreover, the expression for the flow velocity from linear theory is also formulated in this chapter. Finally, the bottom stress values from the present study are compared with the bottom stress values from linear theory and experiment. In conclusion, this model can be used as a different approach for predicting the bottom shear stress in a shallow mine tailings pond. Though we have focused our study on the prediction of the bottom stress in

shallow tailings pond, the mathematical model can be used for prediction of bottom stress in any other shallow or thin-film application.

5.2 Limitations of the model:

There are some limitations of the present model to determine the bottom stress in a shallow tailings pond:

(a) To include the effect of surface tension we have taken that the capillary number value very small which does not match with the real life problems. Just to have an idea how surface tension influences the flow field (flow characteristics or behavior), we have taken a very small capillary number value.

(b) Although by order of magnitude analysis, the terms of $O(\varepsilon^2)$ or higher are neglected but to include the surface tension effect the term of $O(\varepsilon^3)$ is included in the problem formulation.

(c) The study is best suited to shallow or thin-film application, but when the length of a typical shallow tailings pond is too long, this model cannot be used accurately to predict the bottom stress in the pond.

(d) Although we have assumed the flow domain shows laminar behavior but Yang et al. (2008) have described that the flow domain shows turbulent behavior in a tailings pond. Generally shallow tailings pond demonstrates turbulent behavior

under countercurrent flow induced by the wind action. So for better understanding turbulent behavior should be included in a tailings pond which is not accounted in the present study.

(e) The present study considers flat bottom in a tailings pond but in reality the bottom of the tailings pond can be variable. So using a rapidly variable bottom in a tailings pond can better represent the real life problems.

5.3 Future work

The current work has been done as an initial step towards the prediction of bottom shear stress in a shallow mine tailings pond considering viscous and surface tension effects. As an expansion of the current work, the following can be done:

(a) In this study, it was assumed that the bottom of the tailings pond is flat and fixed. But in real life problems, the bottom can be variable. So, using a rapidly variable bottom will strengthen the present mathematical model and better solve the real life problems.

(b) In this work, re-circulation in the tailings pond is neglected. Adding re-circulation will help better to understand the real life problems. Due to mathematical limitations and representation, this is not considered in the present study.

(c) Only the periodic behavior of wind with time is considered in this work, but it can be extended to the periodic behavior with position of the flow domain.

(d) The problem can be extended to a higher order which will give better results, compared to the present results. In this analysis, only the first order solutions are investigated.

(e) Another interesting phenomenon can be investigated, how the wave transfers energy from the surface of the water to the bottom of the pond to cause resuspension. This is not explored in the present study.

(f) Though the prediction of bottom stress in a shallow mine tailings pond is considered in this study, the analysis can be extended to predict the bottom stress in any other shallow or thin-film application.

(g) The analysis is considered to predict bottom stress in water but it can be used for any other fluid, which has a different viscosity than water.

BIBLIOGRAPHY

Acheson, D.J. (1990) Elementary Fluid Dynamics; Clarendon Press: Oxford, 1990

Adu-Wusu, C., Yanful, E.K., & Mian, M.H. (2001). Field evidence of resuspension in a mine tailings pond. Canadian Geotechnical Journal, 38(4):796-808.

Atherton, R.W.; Homsy, G.M. (1976) On the derivation of evolution equations for interfacial waves. Chem. Eng. Commun.1976, 2, 57.

Bailey, M.C., & Hamilton, D.P. (1997). Wind induced sediment resuspension: a lake-wide model. Ecological Bengtsson, L., & Hellstrom, T. (1992). Wind-induced resuspension in a small shallow lake. Hydrobiologia, 241: 163-172.

Benney, D.J (1966). Long waves on liquid films. J. Math. Phys.1966, 45, 150.

Brebner A. And Sangal B.P (1964) A comparison of actual with predicted wave heights and periods for the north shores of lake Ontario and erie.The Engineering Journal.EIC-64.P 32-36

Brourgin, P. 1997 Fluid mechanics of coating processes. Proc. 2nd European Coating Symp. (Euromech 367), Strasbourg, France, pp. 22–25.

Cozar, A., Galvez, J.A, Hull, V., Garcia, C.M., & Loiselle, S.A. (2005).Sediments resuspension by wind in a shallow lake, a model based on turbidimetry. Ecological Modelling, 186: 63-76

CERC (1984).Shore protection manual. U.S. Army Corps of Engineer, Coastal Engineering Research Centre, Vicksburg, M.S.

CERC (2002). Coastal engineering manual. U.S. Army Corps of Engineer, Coastal Engineering Research Centre, Vicksburg, M.S.

CHANG, H. C. (1994), Wave evolution on a falling film, *Ann. Rev. Fluid Mech*. **26**: 103

Dean G.R, Dalrymple A R (1991) Water Wave Mechanics for Engineers and Scientists.

Fenton John. (2010) Coastal and Ocean Engineering.2010

Gaskell P.H, Jimack P. K., Sellier M., Thompson H. M. AND Wilson M. C. T. (2004) Gravity-driven flow of continuous thin liquid films on non-porous substrates with topography. J. Fluid Mech. (2004), vol. 509, pp. 253–280.

Gedney, Richard T.; and Lick, Wilbert (1972) Wind-Driven Currents in Lake Erie.J.Geophys. Res., vol.77, no.15, May 20, 1972, pp.2714-2723

Grant, W.D., & Madsen, O.S. (1979). Combined wave and current interaction with a rough bottom. Journal of Geophysical Research, 84(C4): 1979-1808

Ippen.A.T (1966) Estuary and Coastal Hydrodynamics. McGraw-Hill Book Company, INC

Jing, L., & Ridd, P.V. (1996). Wave-current bottom shear stresses and sediment resuspension in Cleveland Bay, Australia. Coastal Engineering, Vol.29, pp. 169-186.

Jin, K., & Ji, Z. (2004). Case study: modeling of sediment transport and wind wave impact in Lake Okeechobee. Journal of Hydraulic Engineering, 130:1055-1067

Jonsson, I.G. (1966). Wave boundary layers and friction factors, Proc. 10thConference on Coastal Engineering, Tokyo, Japan, ASCE, 1, pp. 127-148.

Kachhwal, L.K., Yanful, E.K., & Lanteigne, L. (2010). Water cover technology for tailings management: a case study of field measurement and model predictions. Water, Air and Soil Pollution, 214 (1-4): 357-382.

Kachhwal, L.K., Yanful, E.K., & Rennie, C.D. (2012). A semi-empirical approach for estimation of bed shear stress in a tailings pond. Journal of Environmental Earth Sciences. 66:823–834

Kalliadasis, S., Bielarz, C. & Homsy, G. M. 2000 Steady free-surface thin film flows over topography. Phys. Fluids 12, 1889.

Khayat Roger E, Siddique Mizanur R. (2002) Influence of inertia and topography on thin-Cavity flow. Physics of Fluids.Vol:14, No: 5.

Kistler, S. F. & Schweizer, P. M. 1997 Liquid Film Coating. Chapman & Hall.

Kizito J. P., Kamotani Y., Ostrach S. (1999) Experimental free coating flows at high capillary and Reynolds number. Experiments in Fluids 27 (1999) 235-243

Lick Wilbert (1976) Numerical modelling of lake currents. Annual review of Earth Planet.1976.

Luettich, R.A., Harleman, D.R.F., & Somlyody, L. (1990). Dynamic behaviour of suspended sediment concentrations in shallow lake perturbed by episodic wind events. Limnology and Oceanography, 35:1050-1067

Mathews K, Noye J, Bills P, 1996-A new method for numerical representation of the land-water boundary in lake circulation models, Elsevier Science Inc, (1996)

Mazouchi, A. & Homsy, G. M. (2001) Free surface Stokes flow over topography. Phys. Fluids 13, 2751

MEND Manual (2001).Prevention and control, Volume 4, Energy Mines and Resources Canada.

Mian, M.H., & Yanful, E.K. (2003).Tailings erosion and resuspension in two mine tailings ponds due to wind waves. Advances in Environmental Research, 7, 745-765.

Mclerney D., Teubner M., Noye J., 2010 -A second order analytical solution for oscillatory wind-induced flow in an idealized shallow lake, Computers and fluids.39:1500-1509(2010)

Mohamed, A, Yong, R., Caporuscio, R and Li, R. (1994) Flooding of a mine tailings site and suspension of solids – Impact and Prevention. 1994. MEND Report 2.13.2b

Myers T.G (1998) SIAM Rev.Society for industrial and Applied Mathematics .Vol 40, No: 3.pp 441-462.

O'Brien S.B.G, Schwartz L.W (2002) Encyclopedia of Science and Colloid science

Oron A, Davis S. H, and Bankoff S.G, (1997) Long-scale evolution of thin liquid films, Rev. Mod. Phys. **69**, 931 ~1997

Pickens, M.K., and Lick, W.J. (1992). Transport and fate of drilling muds. In Proceedings of the 2nd International Conference on Estuarine and Coastal Modelling, Tampa, Florida. pp. 202–214.

Plate EJ (1970) Water surface velocity induced by wind shear. ASCE J Eng Mech Div 96(EM3):295–312

Pritchard, W. G., Scott, L. R. & Tavener, S. J. (1992) Numerical and asymptotic methods for certain viscous free-surface flows. Phil. Trans. R. Soc. Lond. A 340, 1–45.

Quick, M.C., Kingston, K., & Lei, S. (1987). Onset of sediment motion under waves and currents. Canadian Journal of Civil Engineering, 14: 196-206.

Rodney, M.W., & Stefan, H.G. (1987). Conceptual model for wind generated sediment resuspension in shallow ponds. Proceedings National Symposium on Mining, Hydrology, Sedimentology, and Reclamation. University of Kentucky, 263-269

Ruchak J. Kenneth &Weinstein J.Steve Thin-Film Flow at Moderate Reynolds Number. Transactions of the ASME.774 **Vol**. 122, DECEMBER 2000

Samad, M. A., & Yanful, E.K. (2005). A design approach for selecting the optimum water cover depth for subaqueous disposal of sulfide mine tailings. Canadian Geotechnical Journal, 42, 207-228.

Sheng, Y.P., & Lick, W. (1979). The transport and resuspension of sediments in a shallow lake. Journal of Geophysical Research, 84(C4), 1809-1826.

Sorenson R.M (2006) Basic coastal Engineering. Third edition. Springer.

Spillane KT, Hess GD (1978) Wind-induced drift in contained bodies of water. J Phys Oceanography 8:930–935

Stillwagon, L. E. & Larson, R. G. (1988) Fundamentals of topographic substrate levelling. J. Appl.Phys. 63, 5251–5228.

Stone H.A (2002) Nonlinear PDE's in Condensed Matter and Reactive Flows, 297-312.

Tsanis I.K&Saied U. (2005) A wind driven Hydrodynamic and pollutant transport model. Global NEST Journal, Vol 9, No 2, pp 117-131, 2007

Tuck, E.O.; Schwartz, L.W. (1990) A numerical and asymptotic study of some third-order ordinary differential equations relevant to draining and coating flows. SIAM Rev. 1990, 32, 453–469.

Venkatesan K. and Shivpuri R.(1995) Numerical simulation and comparison with water modeling studies of the inertia dominated cavity filling in die casting, Simulation

of Materials Processing: Theory, Methods and Applications, edited by S. F. Shen and P. R. Dawson ~Balkema, Rotterdam,1995, p. 1203.

Wu, J., & Tsanis, I.K. (1995). Numerical study of wind induced water currents. Journal of Hydraulic Engineering, ASCE, 121(5), 388-395.

Wu J (1968) Laboratory studies of wind-wave interactions. J Fluid Mech 34:91–111

Whitehouse, R.J.S., Soulsby, R.L., Roberts, W., and Mitchener, H.J. (1999). Dynamics of estuarine muds-a manual for practical applications. T. Telford, London. Report SR 527HR, Wallingford.

Yanful, E.K., & Catalan, L.J.J. (2002). Predicted and field measured resuspension of flooded mine tailings. Journal of Environmental Engineering, ASCE, 128(4), 341-351.

Yanful, E.K., Samad M. & Mian, M.H. (2004) Shallow water cover technology for reactive sulphide tailings Management.Geo technical news (2004)

Yang, Y. (2001). Wind induced countercurrent flow in shallow water. Ph.D. Thesis, The University of Western Ontario, London, ON.

Yang Y., Straatman A. G., Hangan H., Yanful E.K.(2008) An engineering model for countercurrent flow under wind-induced waves and current. Environ Fluid Mech (2008) 8:19–29

VITA

Name: Md Mahmudur Rahman Faisal

Post-secondary Education   Bangladesh University of Engineering & Technology
and Degrees: 2004 – 2009, B.Sc. (Mechanical)

                                            The University of Western Ontario, London, Ontario,
                                            Canada
                                             (2010 – 2012), M.E.Sc. (Mechanical)

Related work Experience: Research and Teaching Assistant
                                            The University of Western Ontario, London, Ontario,
                                            Canada (2010 – 2012)

Activities/   Councilor of SOGS (Society of Graduate Students), UWO.
Conferences: (2011-2012)

                                            VP External of GES (Graduate Engineering Society),
                                             UWO.(2011-2012)

                                            61st Canadian Chemical Engineering conference, London
                                             Ontario. October 2011

Publications:
                                            Md Mahmudur Rahman Faisal, Roger E.Khayat, Ernest
                                            K.Yanful. Analytical bottom stress determination in
                                            shallow mine tailings pond. 61st Canadian Chemical
                                            Engineering Conference, London, Ontario. October 2011